University of Wisconsin Milwaukee
UWM Digital Commons

Theses and Dissertations

5-1-2014

Damage Detection of Mixed-Mode Cracks in Large Truss Structures Using Wavelet Transform

Hussain Altammar
University of Wisconsin-Milwaukee

Follow this and additional works at: https://dc.uwm.edu/etd

 Part of the Civil Engineering Commons, and the Mechanical Engineering Commons

Recommended Citation

Altammar, Hussain, "Damage Detection of Mixed-Mode Cracks in Large Truss Structures Using Wavelet Transform" (2014). *Theses and Dissertations*. 393.
https://dc.uwm.edu/etd/393

This Thesis is brought to you for free and open access by UWM Digital Commons. It has been accepted for inclusion in Theses and Dissertations by an authorized administrator of UWM Digital Commons. For more information, please contact scholarlycommunicationteam-group@uwm.edu.

DAMAGE DETECTION OF MIXED-MODE CRACKS IN LARGE TRUSS STRUCTURES USING WAVELET TRANSFORM

by

Hussain Altammar

A Thesis Submitted in

Partial Fulfillment of the

Requirements for the Degree of

Master of Science

in Engineering

at

The University of Wisconsin-Milwaukee

May 2014

ABSTRACT

DAMAGE DETECTION OF MIXED-MODE CRACKS IN LARGE TRUSS STRUCTURES USING WAVELET TRANSFORM

by

Hussain Altammar

The University of Wisconsin-Milwaukee, 2014
Under the Supervision of Professors Anoop Dhingra and Sudhir Kaul

The use of dynamic response in damage identification has been gaining considerable attention over the last two decades. The aim of these methods is to detect the presence of a defect or a crack in components or structures. This study focuses on using modal properties for the damage detection of mixed-mode cracks in truss structures. The behavior of a mixed-mode crack is simulated by developing a macroscopic model that is integrated with the finite element model of a truss structure. The modal properties obtained from the model of the damaged structure are found to be comparable to the results of the continuous system model. The direct use of modal properties such as natural frequencies and mode shapes is investigated for simple and large truss structures. It is observed that the traditional approach of using modal properties in damage detection is limited to simple structures with relatively large cracks. Therefore, a damage detection algorithm that uses the wavelet transform is developed in this study. Multiple analyzing wavelets are investigated to enhance the capability of using mode shapes for extracting salient information related to specific damage characteristics. The proposed algorithm is found to be effective and reliable in detecting relatively small mixed-mode cracks even in the presence of noise. The influence of multiple parameters

such as number of truss members, truss member orientation, crack size, crack orientation, etc. is investigated through the application of the proposed algorithm to the Warren truss and the Howe truss structures. The amplitude of wavelet coefficients at a predefined damage location is found to be related to crack size, therefore allowing an evaluation of damage severity. The parameters associated with damage characteristics and geometrical properties are found to be very influential in damage detection, especially when the structure is large and complex.

© Copyright by Hussain Altammar, 2014
All Rights Reserved

To my parents

TABLE OF CONTENTS

LIST OF FIGURES

LIST OF TABLES

ACKNOWLEDGEMENTS

First of all, I would like to express my thanks and appreciation to my advisors, Dr. Anoop Dhingra and Dr. Sudhir Kaul for giving me this great opportunity to grow as a researcher. I would like to thank them for their time, support, and guidance throughout this study. Without their help, this thesis would not have been possible. Also, I would like to thank my committee members, Dr. Rani El-Hajjar, and Dr. Ilya Avdeev for serving on my thesis committee and for their comments and suggestions.

I would like to express special thanks to my family. I would like to thank my beloved parents, my sisters, and my brothers for their continuous support and encouragement with their faithful prayers for my success. Also, I am very thankful to my beloved wife Sukinah for her sincere support all the time and for all the sacrifices that she had made for me. Finally, I want to express my appreciation for my daughter Joud for her smiles that give me hope and energy at difficult moments.

Chapter 1

Introduction

The existence of damage, flaws and cracks in mechanical systems and civil structures presents a serious threat to the life expectancy of these systems. Furthermore, the presence of damage can affect the performance of these systems and influence structural integrity of other associated parts. Successful early detection of cracks can allow engineers enough time to make judicious decisions about the status of a structure. Decisions about repairing certain parts while the structure is in operation, or forcing a structure to be temporarily out of service, or retiring the structure altogether can be made if early detection is successful. This can potentially avoid many undesirable failures of damaged structures that may lead to dangerous consequences pertaining to public safety and major economic losses. An effective detection technique can, therefore, act like an early maintenance alert system.

Cracks that are commonly encountered in engineering structures may be caused by manufacturing processes, overloading from extreme events, aging, unforeseen loading events, or other reasons. Critical structures can be inspected periodically using a rigorous visual inspection. This is one of the oldest and most common nondestructive examination (NDE) techniques for damage identification. Human inspection, however, is vulnerable to errors, and can be inconsistent while being limited to surface inspection only. Other NDE techniques such as thermal field methods, ultrasonic methods or acoustic emission are also constrained since they are limited to the accessible areas of the part being tested, and these techniques often require prior knowledge of the damaged region [1]. These methods are primarily used to obtain more information about

damage characteristics, and to get a better assessment of damage location. Chapter 2 of this thesis discusses some of the existing NDE techniques in detail.

A significant amount of research has been done over the last two decades in order to develop alternative NDE techniques that can overcome the limitations of the conventional experimental methods. The primary goal of these efforts has been to accurately detect the presence of damage at an early stage, and to quantify the damage severity reasonably well [2]. It may be favorable for the detection technique to use the vibration properties of a structure that are induced by the ambient or operating loads rather than measurable excitation loads. However, it is necessary that a damage detection technique should be effective and reliable for large and complex structures with various possible crack (or damage) characteristics. A detection technique also needs to be robust so as to withstand data collection inaccuracies and noise effects, and at the same time it should be easy to implement in practical applications with minimal cost requirements. The need to examine large and complex structures has led to the investigation of the dynamic response of a structure, and the examination of modal properties to develop NDE techniques. Modal properties such as natural frequencies, mode shapes, and strain (curvature) modes have been investigated for damage detection in the existing literature. The presence of a crack-like damage in a structure causes changes in the vibrational properties and the modal response. Detection of these changes heavily relies on the characteristics of the damage and the techniques used to extract the salient information that may be hidden in the modal properties.

This thesis seeks to answer the following questions:

1. What is the influence of mixed-mode cracks on axially loaded components? How are mixed-mode cracks different from purely Mode-I cracks?

2. Can natural frequencies and mode shapes be used to diagnose damage in truss structures? If so, how? Also, what is the influence of multiple parameters on damage detection?

3. Can a damage diagnostic algorithm be proposed for large and complex truss structures? If so, is the damage detection algorithm robust to noise effects?

1.1. Scope of Thesis

This study focusses on using modal properties as the primary diagnostic parameter in truss structures in order to develop a damage detection algorithm. Mixed-mode cracks are particularly investigated since these are commonly present in structural applications. Simple structures are initially considered to validate the FE model. This model is subsequently used to simulate large and complex truss structures by using the continuous (spectral) method to obtain modal properties for comparison. The specific modal properties that are investigated in this study are natural frequencies and mode shapes. Damage introduced in the structure is modeled by using Linear Elastic Fracture Mechanics (LEFM) theory to derive a macroscopic model based on the use of the stress intensify factor. The equivalent macroscopic model that is a function of geometrical properties characterizes a mixed-mode crack that combines Mode-I and Mode-II. The wavelet transform is used in conjunction with statistical measures to develop a damage detection algorithm that can identify damage characteristics. The proposed algorithm is used to investigate the influence of modal parameters on the process of damage detection in various sizes of truss structures. The specific parameters that are considered in this study are as follows: number of truss members, truss member orientation, location of damaged members within the structure, crack size, crack orientation, and crack location within member length. Damage severity is also

investigated in the analysis through the establishment of a relationship with the amplitude of wavelet coefficients.

1.2. Overview of Thesis

This section provides an overview of the entire thesis document. Chapter 1 discusses the significance of this study and presents the research questions that this thesis seeks to answer. The relevance of this study to detecting damage in mechanical components and civil structures is discussed along with promising features that are expected to be associated with the proposed detection technique. The scope of this thesis as well as an overview of all chapters is presented in this chapter.

In Chapter 2, multiple NDE techniques are presented briefly along with their associated properties and their application in damage detection in machines and structures. Some research efforts pertaining to direct use of the modal properties for damage detection are discussed from a theoretical and a practical perspective. Some of the existing literature involving the use of the wavelet transform in damage identification techniques is also discussed to present the capabilities of this unique tool, and its relevance to this study. Various methods used in damage detection, and damage localization, for large and complex structures are presented with examples. Some numerical and experimental examples are also investigated to validate the proposed techniques. Finally, the ability to detect damage severity is also evaluated in a large body of literature using several techniques. Some of these techniques are discussed in the literature review for this study.

Chapter 3 presents the model and analytical results used for simulating damage in a truss structure with an edge crack. A macroscopic model is developed to represent a mixed-mode crack, and this model is integrated with a FE model as well as a continuous model for validation. A numerical example is presented to discuss model validation.

Other numerical examples are also presented to examine the effectiveness of the traditional approach in using the modal properties. Damage detection in simple structures with varying model parameters such as crack size, crack orientation, truss member orientation, etc. are is also investigated. The findings from the analysis performed in this chapter have led to the development of a detection technique that is presented in the next chapter.

In Chapter 4, a damage detection algorithm based on the Continuous Wavelet Transform (CWT) is developed to use the modal properties in detecting and localizing structural damage. The selection process of the algorithm parameters associated with the analyzing wavelet, filtering window and statistical measures is presented along with numerical examples. An outline of the developed algorithm is presented and the application of the algorithm is tested through a numerical example by detecting mixed-mode cracks in a triangular truss structure.

In Chapter 5, the damage detection algorithm is applied to large and complex truss structures to evaluate the capability and robustness of the algorithm in detecting mixed-mode cracks that are simulated by using a macroscopic model. The Warren truss and the Howe truss structures are used with several damage cases to investigate the influence of specific parameters on the performance of the developed algorithm. Some of the parameters that are incorporated in this study are number of truss members, location of damaged members, truss member orientation, crack size, etc.

Chapter 6 concludes the thesis by summarizing the main findings of this study. The outcome of the multiple numerical examples is also briefly discussed in this chapter. Some essential follow-up work is outlined for future research. Potential improvements to the damage detection algorithm and validation testing of the proposed technique are also briefly discussed in this chapter.

Chapter 2

Literature Review

The existing literature consists of several nondestructive damage identification methods that are based on the use of structural modal response. Some of these techniques have been implemented so as to improve the accuracy and reliability of damage diagnostics involving detecting, localizing, and evaluating damages that are commonly encountered in mechanical components and engineering structures. The static and dynamic response of a structure has been utilized to identify parameters that can be used to evaluate structural integrity [2]. This chapter discusses some of the nondestructive examination techniques (NDE) including damage detection techniques that are based on the direct use of modal properties that have been presented in the existing literature. Some of the features associated with these techniques are briefly discussed. Research results involving the study of the capability of the wavelet transform are also assessed in this chapter. The discussion in this chapter includes damage identification techniques that make use of wavelet transform-based methods, optimization algorithms, etc. to detect the presence of damage in large and complex structures.

2.1. Damage Detection Using Nondestructive Testing

Nondestructive testing methods for damage identification have become increasingly important in order to ensure structural integrity and also prevent failure. These methods include visual inspection, acoustic emission, guided wave, infrared emission, vibration analysis, etc. Visual inspection method is often the first step in the examination process to identify a problem, and thus is used in conjunction with other techniques for further analysis. In fact, this method includes more than the use of the naked eye but rather

includes other senses to evaluate damage that can be assessed by an experienced inspector [3]. Many NDE techniques have been developed in research laboratories but only a few of these methods have made the transition from the research phase to the application phase [4]. Acoustic emission (AE) has become a major NDE technique for civil engineering applications, using high frequency sound waves that are emitted by crack propagation and plastic deformation. This technique exhibits high sensitivity and is primarily used to obtain detailed characteristics of damage severity and location [5]. The generation of AE requires a certain amount of stress to be applied to a structure to identify damage characteristics. The application of the AE method to complex geometrical structures can be challenging because of some difficulty associated with data interpretation [4].

Another NDE technique that is widely used to evaluate structural integrity is infrared (IR) emission that measures the distribution of temperature changes caused by a cyclic load that is intentionally applied to the structure for analysis. Thermal analysis obtained from this technique can be utilized to detect areas of stress concentration caused by the presence of a crack, even in complex structures [6]. Another technique called as the guided wave method has been developed recently and is classified as an ultrasound NDE technique. The guided wave is integrated with piezoelectric (PZT) sensors and actuators to obtain the wave speed signal based on the pulse-echo configuration before and after inflicting damage. This technique was implemented by Yuan and Peng [7]. This method is fundamentally different from conventional ultrasonic testing method since it uses low ultrasonic frequency that allows an examination of a larger range for detection. However, the quality of the results obtained from the guided wave method heavily relies upon the geometry of the structure. This method has been commonly used in simple large structures such as pipelines, rail tracks and plate structures [8].

Over the last three decades, vibration analysis has been investigated as a possible NDE technique. Dynamic response of a structure is used as the primary input by using measurement sensors such as accelerometers. Such methods capture the natural frequencies and mode shapes, this will be further discussed in the subsequent section. Bens et al. [4] conducted a detailed review of current NDE testing methods that are available for inspection and evaluation to check the integrity of mechanical components and civil infrastructure.

2.2. Damage Detection Using Modal Properties

The traditional use of modal properties such as natural frequencies and mode shapes has been investigated for damage diagnostics in machines and structures. A comprehensive literature review for natural frequency-based methods in detecting and localizing damage was conducted by Salawu [9]. Damage detection through an examination of the change in natural frequencies was performed in order to provide a global and local damage detection method. It was found that higher vibration modes were often associated with higher sensitivity to a local damage [9]. Cawley and Adams [10] used the ratio of frequency changes for two mode shapes that were found to be independent of frequency in order to detect a defect or a damage. For damage detection, multiple frequency measurements are required in conjunction with a full analysis of all possible damage sites for each type of structure. It was found that this method is computationally expensive to capture every possible damage scenario, even for a simple structure. Stubbs and Osegueda [11] carried out a controlled laboratory experiment for cantilevered specimen to validate the capability of frequency change-based methods for nondestructive damage detection. The authors were particularly interested in evaluating the capability of the method in detecting the crack with varying sizes and locations as well as evaluating its capability in estimating damage severity. It

was concluded that as the damage severity decreases, the method can detect the actual damage but it also predicts incorrect damages at locations at which no damage was introduced.

The vibration modes were investigated by Rizos et al. [12] to examine their capability to detect and locate the presence of the damage in a cantilever beam. The authors combined a continuous cracked beam model with an edge-crack model that was represented through fracture mechanics methods in order to represent local compliance in the structure. It was observed that the absolute difference between the analytical and experimental results decreases as the crack location moves closer to the fixed end. Chondros and Dimarogonas [13] derived the continuous beam model with a transverse edge-crack simulated as a continuous flexibility as well as lumped flexibility for comparison with the experimental results. The findings indicated that continuous flexibility formulation is a better representation of the damage. The authors [14] also compared the results of frequency change between an open crack and a breathing crack for identical crack depth ratios experimentally. The results revealed that a breathing crack is more difficult to detect. A significant amount of research has been conducted over the last two decades on this subject, and has been summarized by Diamarogonas [15].

From a practical standpoint, measuring and tracking natural frequency change is relatively easy and can be accomplished with very few equipment and at a low cost. Also, these measurements are reliable and robust. However, natural frequencies can significantly depend on ambient conditions and boundary conditions [2], and may not change appreciably when the damage is small. It can be concluded from the existing literature that a typical application of modal properties as diagnostic parameters is not viable for large and complex structures since these parameters are not sufficient to yield

a unique indication of the presence of damage, and the specific location of this damage [9, 1].

2.3. Damage Detection Using Wavelet Transform

Recently, wavelet transform has been used for damage diagnostics due to an inherent ability to detect discontinuities resulting from a damage or a crack from the dynamic response of a structure. Liew and Wang [16] used the wavelet transform to process vibration modes in order to identify the damage location in a simply supported beam with a transverse opening crack. The dynamic behavior of the damaged structure was obtained numerically from the continuous model and the FE model for a comparison of the two models. Surace and Ruotolo [17] were among the first researchers who used the wavelet transform for processing the acceleration data from a damaged cantilever beam. The data was used for detecting the presence of a breathing crack by monitoring the shift in natural frequencies. The influence on local flexibility due to the presence of a crack was derived from the stress intensity factor and incorporated into the FE model. Li et al. [18] presented the application of the wavelet finite element method for crack identification of several combinations of crack sizes and positions. The proposed method required two frequency measurements of the damaged structure to identify the crack size and crack position by finding the point of intersection of the first three natural frequency contour lines, that were generated from the frequency response function for all possible damage scenarios. Wavelet analysis of a simply supported beam with an open crack was performed by using various models by Parkrashi et al. [19]. The first mode shape and the static deflection response of the structure were used for damage detection. The authors investigated the influence of the scale factor on wavelet coefficients while varying crack depth ratios and crack locations. The severity of the damage was quantified using a wavelet-kurtosis technique that primarily relied on the

sensitivity of the mode shape to the damage caused by the presence of a crack. Kaul [20] applied a diagnostic technique using various wavelet families on damaged beams with an edge-crack by varying crack sizes and locations. The proposed diagnostic technique made use of skewness and kurtosis parameters of the damaged beams as well.

Chang and Chen [21] and Zhong and Oyadiji [22] investigated the presence of multiple cracks in beam-like structures for damage detection using the wavelet transform, and found that discontinuities due to the presence of cracks can be efficiently detected even when the distance between the cracks is very small. Chang and Chen [21] made use of the continuous wavelet transform (CWT) for detection of multiple cracks that were represented by a rotational spring. It was observed that larger peak values of wavelet coefficients were obtained when the crack is located near the fixed joint, while the opposite effect was observed near the free end. Zhong and Oyadiji [22] presented the use of stationary wavelet transform (SWT) in a simply supported beam. The authors particularly investigated the influence of crack depth, crack width, and sampling distance on the signal resolution of the SWT for damage diagnostics. The proposed method was able to de-noise the data and detect small cracks even up to a crack ratio of 4%. It was concluded that the magnitude of the absolute maximum coefficients decreases as the crack width increases. The CWT with the use of the Gaussian wavelet was used for processing numerical and experimental results by Rucka [23] to study the application of the higher order mode shapes in damage detection. It was observed that for higher modes with a lower number of vanishing moments, the magnitude of the wavelet coefficients is higher at the predefined crack location, indicating that higher modes are more sensitive to the presence of damage [21, 23]. In addition, the effectiveness of using mode shapes in capturing a discontinuity due to the

presence of a crack in the spatial wavelet transform was demonstrated to depend on the mode order.

2.4. Damage Identification in Complex Structures

Several damage detection techniques have been investigated for large and complex structures using numerical as well as experimental studies in the existing literature [24-33]. Nair and Kiremidjian [24] used natural frequencies and mode shapes to develop a global damage sensitivity feature based on the wavelet transform of acceleration signals to monitor the change in measurements between damaged and undamaged structures. An ASCE benchmark structure was simulated numerically and experimentally with various damage patterns by removing and cutting braces, and loosening some of the bolts in the structure. The proposed approach was found to be incapable of detecting local damage caused by loosening bolts. A global damage detection algorithm that is based on a parameter estimation method of mode shapes was proposed by Pothisiri and Hjelmstad [25] for damage detection in complex truss structures. A truss bridge was modeled with several damage cases using a finite element (FE) model to identify damaged members by using an element-group updating algorithm. It was concluded that some truss members are more sensitive to damage in specific regions within the structure. This conclusion was also verified experimentally by Kim and Bartkowicz [26] by using an optimal updating method for global damage detection, and a design sensitivity method for identification of damaged truss members of a hexagonal truss. Several damage cases were not successfully identified because the proposed approach required a significant change in the dynamic modal response between undamaged and damaged structures.

Weber and Paultre [27] presented damage identification of a laboratory-size truss tower using a sensitivity-based algorithm. A damage simulated by removing members at

different locations was successfully localized, and the extent of the damage was accurately quantified. A vibration-based damage detection method presented by Hao et al. [28] incorporated a genetic algorithm to obtain the global optimum by comparing the measured vibration data collected before damage with data collected after a damage is inflicted on the structure. To identify the location and magnitude of the damage, the changes in the measurements were matched as closely as possible with the FE model of the structure through a model updating technique. Multiple damage configurations introduced in a plane frame consisting of three members were identified using the changes from both natural frequencies and mode shapes. However, the robustness and reliability of this optimization method relies heavily upon the weight factor that needs to be determined iteratively for each type of structure through the use of the forward problem.

Local damage detection of frame structures was demonstrated by Ovanesova and Suarez [29] for the application of the wavelet transform to an entire structure. The static and dynamic response of the damaged structure obtained from multiple simulations was used for detection of discontinuities through the application of several families of wavelets. It was found that the boundary effects due to a support or a corner joint in the wavelet spatial domain were often significant and could cause problems with damage detection. The static response of a damaged structure was used for detecting damage through the use of the wavelet transform by Wang et al. [30]. The damage simulated in truss-like structures by reducing the cross sectional area at a predefined element was detected through numerical and experimental methods. The proposed technique was successfully applied to a complex structure by utilizing the response signals of the undamaged and damaged structure. Li et al. [31] derived a modal strain energy decomposition method that was developed from the modal strain energy method proposed by Stubbs et al. [32] for damage identification of individual members in a

structure. The proposed method is based on decomposing the modal strains of each member into longitudinal and transverse strain energy components for the undamaged and damaged structural response, yielding two damage indicators. In order to evaluate the capability of the method, two FE models of a three dimensional five-story frame structure and a complex offshore platform were constructed to identify the location of the damaged members, and also to estimate the damage severity from various damage scenarios. It was found that the damage occurring in horizontal members was detected by a major contribution of the axial damage indicator and vice versa. However, the proposed technique did not estimate the damage severity very well. Tang et al. [33] proposed a damage identification method based on the octonion structural response vector that consists of static strains at specific locations and natural frequencies of a structure. The implementation of the method was demonstrated on a FE model of a large simply supported beam with a transverse open crack. For damage detection, the proposed method made use of the structural health monitoring data that was collected a priori at different periods of time.

2.5. Conclusions

From the literature review discussed in this chapter, it is found that the traditional use of modal properties is not expected to give a strong indication of the existence of damage in large structures. It can also be concluded from the existing literature that a majority of the methods used for damage detection in large and complex structures have several shortcomings. For example, the need for the structural response of the undamaged and damaged structures, requirement of a high level of damage severity, lack of local damage indication, etc. are some of the issues associated with the damage detection methods. However, the wavelet transform is recognized as a promising technique for damage identification that can be based on vibrational response.

Based on the findings from the literature, this study investigates the development of a damage detection algorithm for truss structures by using the modal properties in conjunction with the wavelet transform. The damage inflicted in the truss structures, used in this study, is a combination of Mode-I and Mode-II cracks, commonly called as a mixed-mode crack in the literature. The mixed-mode crack is modeled by a macroscopic spring element. The modal properties of the damaged truss structure are verified in multiple steps by using a continuous cracked bar and a FE model. The traditional use of modal properties is also investigated in Chapter 3. A damage detection algorithm that integrates the wavelet transform and uses some statistical measures is developed in Chapter 4 to overcome the limitations related to the traditional approach. The application of the proposed algorithm is demonstrated through damage detection in large truss structures presented in Chapter 5.

Chapter 3

Structural and Damage Simulation

Mathematical modeling and simulation plays an essential role in the analysis of structures that need to withstand multiple loading configurations under varying conditions. Mathematical modeling can significantly mitigate the need for carrying out expensive experimentation and validation testing. Accurate simulation can be a challenging task for complex structures, requiring extensive information about boundary conditions, material properties, etc. in addition to a holistic understanding of a problem that an analyst is attempting to solve. This chapter focuses on modeling of a truss structure with a mixed-mode crack using the principles of Linear Elastic Fracture Mechanics (LEFM). This is done by developing a finite element (FE) model of a cracked bar initially. The results of the FE model are compared to a continuous cracked bar model for validation. After validation, the FE model is extended to triangular truss structures. Two examples are presented in this chapter to validate the results of the FE model. An additional example is presented to investigate the use of modal properties such as natural frequencies and mode shapes in detecting and localizing the damage caused by the presence of the mixed-mode cracks in a structure. This chapter concludes by summarizing the observations with regards to the effectiveness of the FE model as well as the modal properties for the purposes of damage detection.

3.1. Scope of Fracture Mechanics

A significant number of structural failures are initiated from the presence of a high stress concentration in the vicinity of crack-like defects. These defects nucleate into cracks and propagate further with an increasing crack size, leading to plastic yielding failure or sudden brittle fracture. It is essential to obtain a quantitative measure of the

resistance of a cracked material to brittle fracture. LEFM is a useful approach that can be used to comprehend the effects of a crack by using a semi-empirical quantity, called as the stress intensity factor (SIF). The stress field near the crack tip is expressed as:

$$\sigma_{r\theta} = \frac{K}{\sqrt{2\pi r}} f(\theta) \tag{3.1}$$

In Eq. (3.1), r and θ represent the polar coordinates with the origin located at the crack tip and K is the SIF. LEFM assumes elastic behavior of the material around the tip to efficiently use and measure SIF. It is assumed that the shape of the crack changes and the crack tip becomes blunted when the material is plastically deformed due to localized plastic strain around the crack tip. As can be observed from Eq. (3.1), a sharp crack will exhibit infinite stress at $r = 0$. To overcome this limitation, a plastic zone size is defined around the crack tip, and a correction factor is used to modify the crack size and incorporate an additional term into the stress field equation [34]. The LEFM approach is applicable when the structure is subject to a load (or stress) that limits the size of the plastic zone in comparison to crack length and cross section dimensions. This study makes extensive use of LEFM. All the limitations of LEFM, therefore, are applicable to the models developed in this study. This implies that a small crack size and a negligible plastic zone are assumed for the purposes of this study.

3.2. Fracture Modes

A cracked structure may be subjected to different types of loading conditions. The geometry of the crack and the applied load are used to determine the prevailing mode of the crack. Three main modes are identified in the literature of fracture mechanics. Mode-I occurs when the crack surface is under a load that is normal to the crack plane. Mode-II crack is defined when the crack surface is subjected to in-plane shear loading that causes the two sides of the crack surface to slide relative to each other. Mode-III is defined as a tearing mode and occurs when applied load causes out-of-plane shear.

Figure 3.1 illustrates the above described modes of fracture, as seen in a structural member with a side (or edge) crack. It may be noted that a mixed-mode crack can results either due to loading conditions or due to crack geometry. This study focuses on the mixed-mode crack resulting from a combination of Mode-I and Mode-II. This combination is often encountered in engineering components and structures.

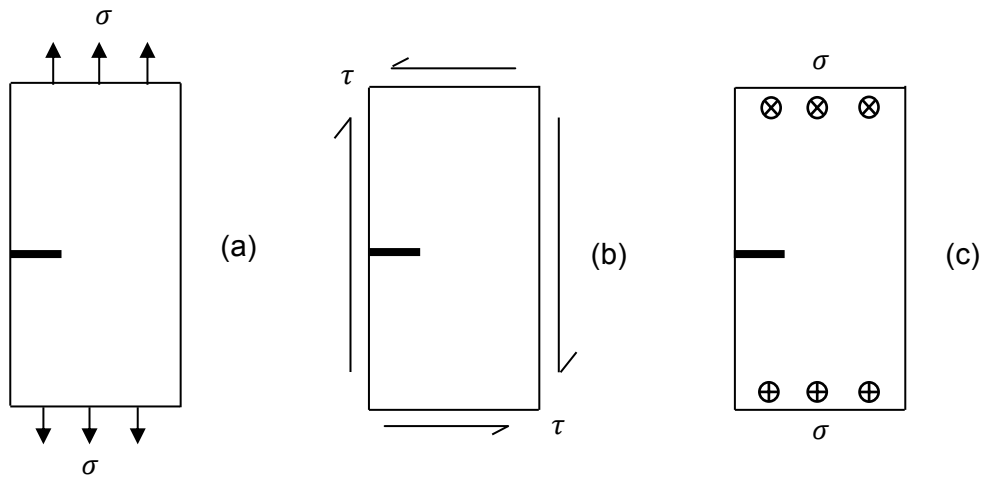

Figure 3.1: Fracture Modes-an Edge Crack (a) Mode-I, (b) Mode-II, And (c) Mode-III. Out of Plane Stress – ⊗; in Plane Stress – ⊕.

Each fracture mode is associated with the stress intensity factor K that characterizes the behavior of the crack based on crack shape, size, and loading configuration. The SIF for each mode is identified distinctly as K_I, K_{II}, or K_{III}. The SIF also provides a means for quantifying the amplitude of crack singularity as well as crack stability. The stress field in the vicinity of the crack tip can be determined in terms of SIF when the cracked structure is subjected to a stress away from the crack location. In isotropic materials, the stress field for Mode-I and Mode-II is expressed [34] as follows:

$$\begin{bmatrix}\sigma_{rr}\\ \sigma_{\theta\theta}\\ \tau_{r\theta}\end{bmatrix} = \frac{K_I}{\sqrt{2\pi r}}\begin{bmatrix}\frac{1}{4}cos\frac{\theta}{2}-\frac{1}{4}cos\frac{3\theta}{2}\\ \frac{3}{4}cos\frac{\theta}{2}+\frac{1}{4}cos\frac{3\theta}{2}\\ \frac{1}{4}sin\frac{\theta}{2}+\frac{1}{4}sin\frac{3\theta}{2}\end{bmatrix} \tag{3.2}$$

$$\begin{bmatrix}\sigma_{rr}\\ \sigma_{\theta\theta}\\ \tau_{r\theta}\end{bmatrix} = \frac{K_{II}}{\sqrt{2\pi r}}\begin{bmatrix}-\frac{5}{4}sin\frac{\theta}{2}+\frac{3}{4}sin\frac{3\theta}{2}\\ -\frac{3}{4}sin\frac{\theta}{2}-\frac{3}{4}sin\frac{3\theta}{2}\\ \frac{1}{4}cos\frac{\theta}{2}+\frac{3}{4}cos\frac{3\theta}{2}\end{bmatrix} \tag{3.3}$$

The stresses are given in polar coordinates and cannot be evaluated unless SIF is determined. As discussed earlier, SIF is determined from LEFM approach as:

$$K_I = \sigma\sqrt{\pi a} f_I(\emptyset) \tag{3.4}$$

$$K_{II} = \tau\sqrt{\pi a} f_{II}(\emptyset) \tag{3.5}$$

In Eq. (3.4) and Eq. (3.5), σ is the normal stress applied away from the crack, τ is the in-plane shear stress applied remotely, a is the crack size, and $\mathrm{f_I}(\emptyset)$ and $\mathrm{f_{II}}(\emptyset)$ are dimensionless factors based on crack shape, geometry and loading configuration. These factors are commonly available for different crack shapes and loading conditions [35].

3.2.1. Mixed Mode Fracture

The mixed mode state of stress discussed in this section combines the opening mode and the shearing mode. An inclined crack is introduced in a plate that is subjected to a far-field normal stress σ as shown in Figure 3.2. The crack is inclined at an angle β, from the vertical edge. It may be noted that if the crack angle equals to 90°, the applied stress is normal to the crack surface, resulting in a pure Mode-I configuration. The SIF for Mode-I, as expressed in Eq. (3.4) is used when the angle is 90°. However, if the angle is between 0° and 90°, the stress field induces combine loading of K_I and K_{II} as expressed in Eq. (3.6).

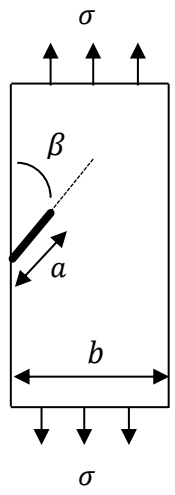

Figure 3.2: Inclined Crack in a Plate Subjected to Uniaxial Stress.

At the tip of the mixed-mode crack, an equivalent expression is required to represent the SIF at any angle. This is done by applying the maximum principal stress criteria to the stress field expressed in Eq. (3.6).

$$\begin{bmatrix}\sigma_{\theta\theta}\\ \tau_{r\theta}\end{bmatrix} = \frac{1}{2\sqrt{2\pi r}}\cos\frac{\theta}{2}\begin{bmatrix}K_I(1+\cos\theta) - 3K_{II}\sin\theta\\ K_I\sin\theta + K_{II}(3\cos\theta - 1)\end{bmatrix} \tag{3.6}$$

Since shear stress at the principal stress is zero, the shear stress from Eq. (3.6) can be used to solve for θ as follows:

$$K_I\sin\theta + K_{II}(3\cos\theta - 1) = 0 \tag{3.7}$$

Using Eq. (3.7) to solve for angle θ that yields the direction in which the crack seeks to propagate, the following expression is derived:

$$\theta_p = 2\tan^{-1}\left[\frac{K_I}{4K_{II}} \pm \frac{1}{4}\sqrt{\left(\frac{K_I}{K_{II}}\right)^2 + 8}\right] \tag{3.8}$$

Eq. (3.8) yields two angles for θ_p, but only one of the two solutions is feasible. Substituting Eq. (3.8) into Eq. (3.6) to compute the principal stress as:

$$\sigma_1 = \frac{1}{2\sqrt{2\pi r}}\cos\frac{\theta_p}{2}\left[K_I\left(1+\cos\theta_p\right) - 3K_{II}\sin\theta_p\right] \tag{3.9}$$

Crack propagation occurs when SIF at the crack reaches or exceeds fracture toughness of the material. The critical stress associated with the fracture toughness is calculated as:

$$\sigma_c = \frac{K_{IC}}{\sqrt{2\pi r}} \tag{3.10}$$

The equivalent SIF can be determined by equating Eq. (3.10) and Eq. (3.9) and solving for K_{IC} as the equivalent SIF even though K_{IC} is used for the opening mode only. The loading for the propagation of the inclined crack is a combination of the opening and shearing fracture modes, but the crack tends to propagate normal to the applied load, that is in pure Mode-I. The equivalent SIF is derived as follows:

$$K_{I,eq} = K_I \cos^3\frac{\theta_p}{2} - 3K_{II}\sin\frac{\theta_p}{2}\cos^2\frac{\theta_p}{2} \tag{3.11}$$

To make the equivalent SIF function of the applied stress, the pure single mode SIFs can be evaluated by resolving the applied stress into two components of normal and shear stress. Substituting the normal stress component in Eq. (3.4) and the shear stress in Eq. (3.5) yield the following:

$$K_I = \sigma \sin^2\beta \sqrt{\pi a} f_I(\emptyset) \tag{3.12}$$

$$K_{II} = \sigma \sin\beta \cos\beta \sqrt{\pi a} f_{II}(\emptyset) \tag{3.13}$$

Substituting single mode SIFs into Eq. (3.11) gives the equivalent SIF for the inclined crack in Figure 3.2.

$$K_{I,eq} = \sigma\sqrt{\pi a}\left[\sin^2\beta\cos^3\frac{\theta_p}{2} f_I(\phi) - 3\sin\beta\cos\beta\sin\frac{\theta_p}{2}\cos^2\frac{\theta_p}{2} f_{II}(\phi)\right] \tag{3.14}$$

In Eq. (3.14), the geometrical factors for opening and shearing mode are expressed [35] as follows:

$$f_I(\emptyset) = 1.122 - 0.231\emptyset + 10.55\emptyset^2 - 21.71\emptyset^3 + 30.382\emptyset^4 \tag{3.15}$$

$$f_{II}(\emptyset) = \frac{1.122 - 0.561\emptyset + 0.085\emptyset^2 + 0.18\emptyset^3}{\sqrt{1-\emptyset}} \tag{3.16}$$

In Eq. (3.15) and Eq. (3.16), $\emptyset = a/b$, a is the crack size, and b is the width of the plate as illustrated in Figure 3.2. Eq. (3.14) characterizes the SIF of mixed-mode crack, as shown in Figure 3.2 for the inclined crack. It may be noted that the SIF is a function of crack depth, crack orientation, loading condition, and geometry of the structure. Furthermore, it may be noted that the orientation of the crack propagation is required in order to compute the SIF in Eq. (3.14). The derivation from this section will be used in the subsequent section to model the mixed-mode (inclined) crack using an approach based on LEFM.

3.3. Crack Modeling

The presence of a crack in a structure introduces an increment in local flexibility that has higher potential strain energy release due to stress concentration at the crack tip. To quantify this flexibility, the crack can be modeled as a linear spring, and the strain energy can be used to compute the spring constant. The model developed herein will be used for structural analysis throughout this study. For a structural member of a truss, the macroscopic model of the crack is characterized as a linear spring using the longitudinal displacement field only, since all members of a truss exhibit extension and or compression. In Figure 3.3, a fixed bar with a rectangular cross sectional area has an edge mixed-mode crack introduced at the top side of the bar. A uniaxial force F is acting upon the bar and is acting away from the boundary or the crack location.

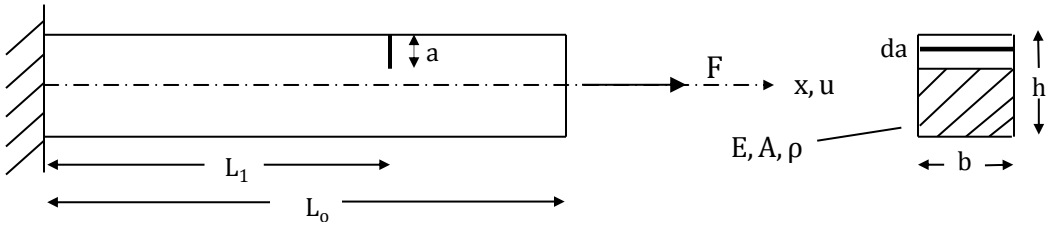

Figure 3.3: Fixed Bar with an Edge Crack Subjected to Axial Load.

The strain energy due to the crack can be evaluated by integrating the equivalent SIF over the surface area of the crack, and is expressed as:

$$\Delta U = \frac{1}{E}\int_0^A K_{I,eq}^2 dA \tag{3.17}$$

In Eq. (3.17), ΔU is the change in strain energy and E is modulus of elasticity, $A = bda$ is the surface area of the crack. The external work induced by the force F is transformed to potential energy at the crack and can be expressed as follows for the spring used for macroscopic modeling of the crack:

$$\Delta U = \frac{F^2}{2k_s} \tag{3.18}$$

In Eq. (3.18), k_s is the spring constant of the linear spring. Equating Eq. (3.17) and (3.18) and substituting the applied stress in terms of force and cross sectional area yields the following:

$$\frac{1}{k_s} = \frac{2\pi}{Ebh^2}\int_0^a \left[\sqrt{a}\left[\sin^2\beta\cos^3\frac{\theta_p}{2} f_I(\phi) - 3\sin\beta\cos\beta\sin\frac{\theta_p}{2}\cos^2\frac{\theta_p}{2} f_{II}(\phi)\right]\right]^2 da \tag{3.19a}$$

Finally, substituting the functions of geometrical factors as a function of $\phi = a/h$ and integrating over crack depth provides the spring constant of the linear spring used to represent the inclined crack. By denoting the integral as G, the stiffness of the crack can be expressed as:

$$k_s = \frac{Ebh^2}{2\pi\sin\beta\cos^2\frac{\theta_p}{2} G} \tag{3.19b}$$

3.4. Modal Analysis – Truss Structure

If a specific member of a structure has a crack or a crack-like damage, the global stiffness of the structure reduces resulting in a drop in natural frequencies. The vibrational modes of the structure may also be affected due to the presence of a crack, showing either local or global distortion depending on crack size, crack orientation, crack location, etc. Thus, a longitudinal vibration characteristic of a truss member with an edge crack may be used to identify crack depth and crack location. In this study, the modal

properties of a structure are extracted using the finite element (FE) method because of its ability to provide a reasonably accurate solution for complex mechanical and structural problems. Furthermore, the FE model can be easily integrated with the macroscopic model of the crack that was discussed in the previous section. This is done by using the linear spring element representing the crack as a connection between the two sides of the structural member on either side of the crack. This model is validated through a comparison of results between the FE model and the continuous model for a bar.

3.4.1. Modal Analysis-Finite Element Model

The equation of motion (EOM) of a structure can be expressed in terms of global matrices as follows [36]:

$$[M]\{\ddot{x}\} + [C]\{\dot{x}\} + [K]\{x\} = \{f\} \tag{3.20}$$

In Eq. (3.20), $\{x\}$ is the displacement vector, $\{\dot{x}\}$ is the velocity vector, $\{\ddot{x}\}$ is the acceleration vector: $[M]$, $[C]$, and $[K]$ are the mass, damping, and stiffness matrices, respectively and $\{f\}$ is the external force vector. By neglecting the damping matrix and with no external force vector, the equation of the undamped system is expressed as:

$$[M]\{\ddot{x}\} + [K]\{x\} = 0 \tag{3.21}$$

The standard solution of the homogeneous system in Eq. (3.21) is given as follows:

$$\{x\} = \{X\}e^{i\omega t} \tag{3.22}$$

In Eq. (3.22), ω is the natural frequency of the structure and $\{X\}$ is natural mode shape matrix. Substituting the results of Eq. (3.22) in Eq. (3.21) yields the following:

$$([K]_{n\times n} - \omega_n^2[M]_{n\times n})\{X\}_{n\times 1} = 0 \tag{3.23}$$

Eq. (3.23) is a set of n linear homogeneous equations with nontrivial solution only if the determinant of the coefficients of natural modes vector is nonzero. Finally, natural

frequencies and natural modes are extracted by finding the eigenvalues and eigenvectors of Eq. (3.23) as:

$$|[K]_{n\times n} - \omega^2[M]_{n\times n}| = 0 \tag{3.24}$$

The solution of Eq. (3.24) gives n natural frequencies, equivalent to the number of degree of freedoms associated with the system. Likewise, the vibrational modes corresponding to each eigenvalue are determined by Eq. (3.23).

The global stiffness and mass matrices are assembled from individual element matrices in global coordinates. Eq. (3.25) represents matrix formulation of the undamaged structure consisting of n elements.

$$\left[K^{(u)}\right]_{n\times n} = \sum_{e=1}^{n}\left[k^{(e)}\right] \qquad \left[M^{(u)}\right]_{n\times n} = \sum_{e=1}^{n}\left[m^{(e)}\right] \tag{3.25}$$

In Eq. (3.25), $\left[k^{(e)}\right]$ and $\left[m^{(e)}\right]$ are stiffness and mass matrices of individual elements constructed in global coordinates which are more convenient for complex structures. Figure 3.4a illustrates the transformation of nodal displacements of an individual element into global coordinates.

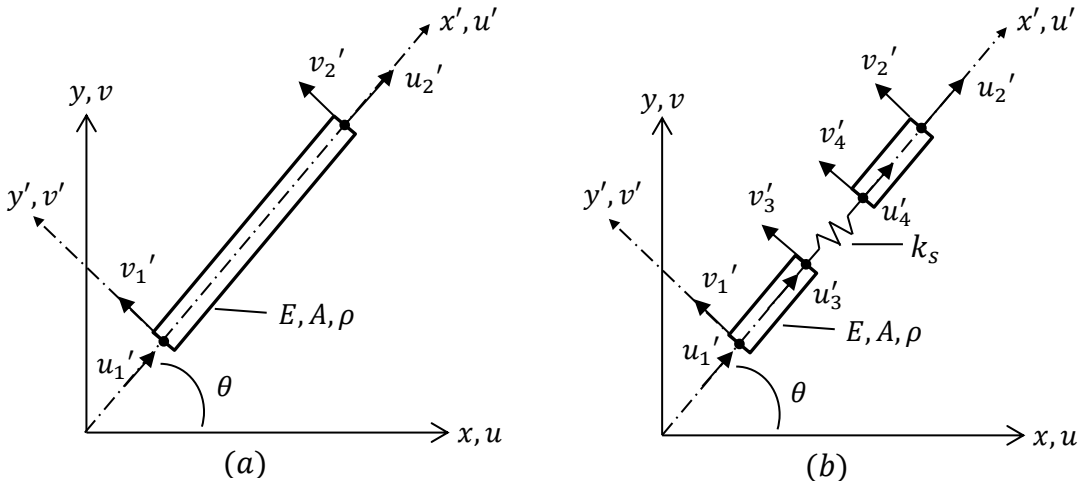

Figure 3.4: (a) Nodal Displacements of Undamaged Truss Member in Global Coordinates of 2-D Plane. (b) Nodal Displacements of Damaged Truss Member with a Spring Element Oriented in the Plane.

The transformation matrix which relates local displacements to global displacements is given in the matrix form as:

$$T = \begin{bmatrix} c & s & 0 & 0 \\ -s & c & 0 & 0 \\ 0 & 0 & c & s \\ 0 & 0 & -s & c \end{bmatrix} \tag{3.26}$$

In Eq. (3.26), $c = \cos\theta$ and $s = \sin\theta$. Therefore, the global stiffness matrix of the bar element that is oriented arbitrary at an angle, θ in the plane is expressed as:

$$[k^e] = [T]^T[k'][T] = \frac{AE}{L}\begin{bmatrix} c^2 & cs & -c^2 & -cs \\ & s^2 & -cs & -s^2 \\ & & c^2 & cs \\ Sym & & & s^2 \end{bmatrix} \tag{3.27}$$

In Eq. (3.27), L is the bar length, A is the cross sectional area of the bar, E is modulus of elasticity of the material, and $[k']$ is the stiffness matrix of bar element in local coordinates. The mass matrix however does not change with the orientation of the bar element, thus the consistent mass matrix in the global coordinates is expressed as:

$$[m^e] = [T]^T[m'][T] = [m'] = \frac{\rho AL}{6}\begin{bmatrix} 2 & 0 & 1 & 0 \\ & 2 & 0 & 1 \\ & & 2 & 0 \\ Sym & & & 2 \end{bmatrix} \tag{3.28}$$

In Eq. (3.28), ρ is material density and $[m']$ is the mass matrix of the bar in local coordinates. For a damaged structure formulation, Figure 3.4b illustrates bar elements separated with a spring element which represents the damage characterized in Section 3.4. The macroscopic model of the crack represented by a spring element also requires to be transformed along with the adjacent elements as:

$$[K_s] = [T]^T[k_s'][T] = k_s\begin{bmatrix} c^2 & cs & -c^2 & -cs \\ & s^2 & -cs & -s^2 \\ & & c^2 & cs \\ Sym & & & s^2 \end{bmatrix} \tag{3.29}$$

The mass of this spring element is assumed to be negligible. Thus, the global stiffness and mass matrices of the damaged structure can be expressed as:

$$\left[K^{(d)}\right]_{n\times n} = \sum_{e=1}^{n+1}\left[k^{(e)}, K_s^{(i)}\right] \qquad \left[M^{(d)}\right]_{n\times n} = \sum_{e=1}^{n+1}\left[m^{(e)}, M_s^{(i)}\right] \tag{3.30}$$

In Eq. (3.30), $K_s^{(i)}$ and $M_s^{(i)}$ are denoted with superscript i to define their locations among other elements in the global matrices. Substitution of Eq. (3.30) into Eq. (3.24) yields the natural frequencies of the damaged structure and the mode shapes showing the effect of the damage can be obtained by using Eq. (3.23).

3.4.2. Modal Analysis-Continuous System Model

To validate the FE model of the damaged structural element, this section discusses the formulation of the continuous model based on the governing equation of motion for a cantilever bar with an edge crack introduced at a distance L_1 from the fixed end as shown in Figure 3.3. The natural frequencies and natural modes are extracted from this model and compared with the results obtained from the FE model. In this formulation, the local flexibility due to the crack is considered as a non-dimensional compliance (inverse of stiffness) that is expressed as:

$$\theta_c = \frac{AE}{k_s L_o} \tag{3.31}$$

The free longitudinal vibration of the bar in terms of axial displacement u and time t is expressed as follows [37]:

$$c^2 \frac{\partial^2 u}{\partial x^2}(x,t) = \frac{\partial^2 u}{\partial t^2}(x,t) \tag{3.32}$$

In Eq. (3.32), variable *c* defined as:

$$c = \sqrt{\frac{E}{\rho}} \tag{3.33}$$

The general solution of longitudinal vibration for Eq. (3.32) is obtained as follows:

$$u(x,t) = \left(C_1 \cos\frac{\omega x}{c} + C_2 \sin\frac{\omega x}{c}\right)(D_1 \cos\omega t + D_2 \sin\ \omega t) \tag{3.34}$$

The constants C_1, C_2, D_1, and D_2 can be determined from applying the boundary conditions. For this case, the axial displacement of the bar is assumed free and independent of time. The local flexibility due to the crack in the bar is dividing it into two segments and the modes of harmonic vibration of each segment can be expressed as:

$$u(x) = \begin{cases} u_1(x) = C_1 \cos\frac{\omega x}{c} + C_2 \sin\frac{\omega x}{c} & for \;\; 0 \le x \le L_1 \\ u_2(x) = C_3 \cos\frac{\omega x}{c} + C_4 \sin\frac{\omega x}{c} & for \;\; L_1 \le x \le L_o \end{cases} \tag{3.35}$$

As can be seen Eq. (3.35), four conditions are necessary to determine the constants. Two boundary conditions from the fixed end and two compatibility conditions at the crack location are stated as follows:

$u(0) = 0 \;\; => u_1(0) = 0$ $\qquad\qquad$ $u'_1(L_1) = u'_2(L_1)$

$u'(L_o) = 0 \;\; => u'_2(L_o) = 0$ $\qquad\qquad$ $u_2(L_1) - u_1(L_1) = \theta_c L_o u'_2(L_1)$

Applying the first boundary condition yields $C_1 = 0$. The other conditions form a set of three equations constructed in the matrix form and a variable g is defined as:

$$g(L_o, L_1, \theta) = \begin{bmatrix} 0 & -\frac{\omega}{c}\sin\frac{\omega L_o}{c} & \frac{\omega}{c}\cos\frac{\omega L_o}{c} \\ \frac{\omega}{c}\cos\frac{\omega L_1}{c} & \frac{\omega}{c}\sin\frac{\omega L_1}{c} & -\frac{\omega}{c}\cos\frac{\omega L_1}{c} \\ -\sin\frac{\omega L_1}{c} & \cos\frac{\omega L_1}{c} + \theta_c L_o \sin\frac{\omega L_1}{c} & \sin\frac{\omega L_1}{c} + \theta_c L_o \cos\frac{\omega L_1}{c} \end{bmatrix} \tag{3.36}$$

The solution of the system of equations in Eq. (3.36) is determined by finding the eigenvalues which are the natural frequencies ω_n of the cracked bar. Then, the natural frequencies can be substituted into Eq. (3.36) to solve for C_3 and C_4 after setting $C_2 = 1$. Once the constants are evaluated, the system of equations of Eq. (3.35) represent the mode shapes over the entire length of the cracked bar.

3.5. Numerical Examples

This section presents three numerical examples to demonstrate the validation of the FE model and to investigate the effectiveness of using natural frequencies and natural

modes for damage identification. Example 1 illustrates results of the FE model and the continuous model for a bar with an edge crack in order to have a quantitative measure of the difference in the predicted natural frequencies and vibrational modes between the two models. Example 2 examines the robustness of the FE model in accurately representing the actual model and its capability to handle more complex structures where the application of the spectral method becomes very challenging. Example 3 is primarily used to examine damage identification based on natural frequencies and mode shapes in localizing damage and estimating the severity of the damage. In this example, a triangular truss with two members with a side crack at predefined location is analyzed in terms of various parameters such as crack size, orientation, member orientation, etc.

3.5.1. Example 1: FE Model vs. Continuous Model of a Fixed Bar

The bar shown in Figure 3.3 is discussed in this subsection. For comparison purposes, the FE model and the continuous model are simulated in MATLAB®. The bar length, L_o, is 18in and the crack is located at 16in, L_1, from the fixed end. The bar has a height, h, of 0.5in and breadth, b, of 0.021in. In terms of material properties, the modulus of elasticity, E, and the material density, ρ, respectively are 10.2 Msi and 0.1lb/in^3.

The models presented in the previous sections are developed in MATLAB® to determine modal properties. The results of both the models are plotted together for a visual comparison. The first three natural frequencies are obtained for the bar with an initial crack size of 0.01in that is increased incrementally up to 0.5in and are plotted in Figure 3.5 through Figure 3.7. The crack orientation, β, is 90^o making the loading purely Mode-I. The crack location, L_1, is also kept unchanged for this example. The first three vibrational modes are obtained for a crack depth of 0.01in and are plotted in Figure 3.8 through Figure 3.10.

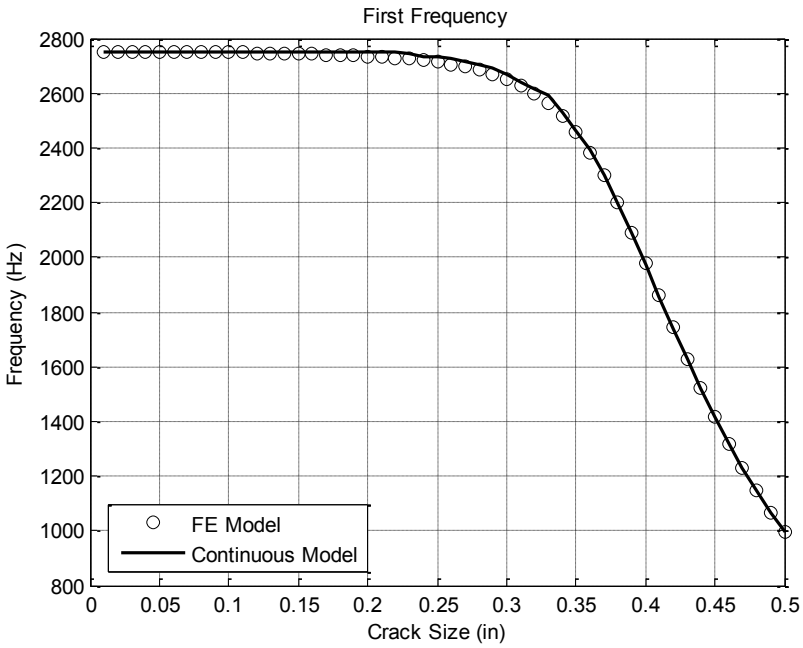

Figure 3.5: First Frequency of the Fixed Bar.

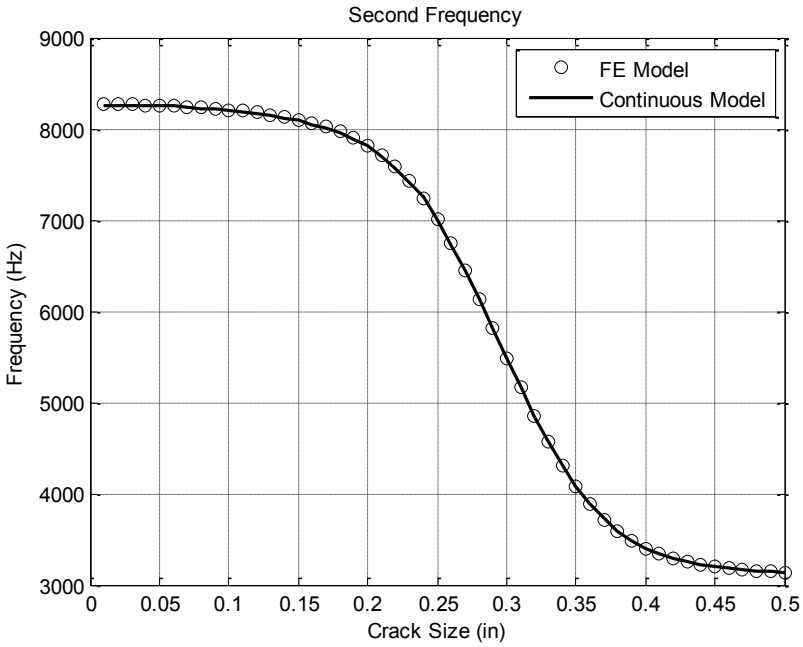

Figure 3.6: Second Frequency of the Fixed Bar.

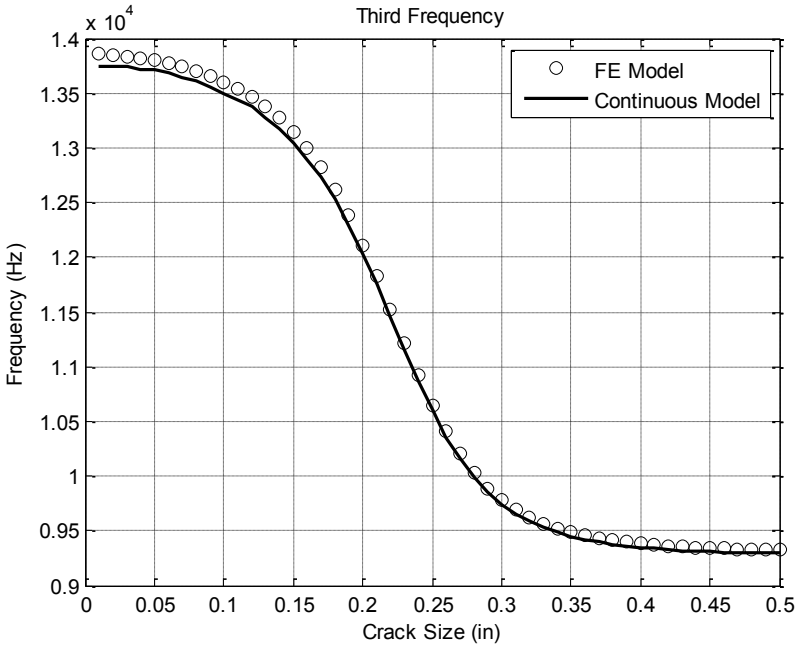

Figure 3.7: Third Frequency of the Fixed Bar.

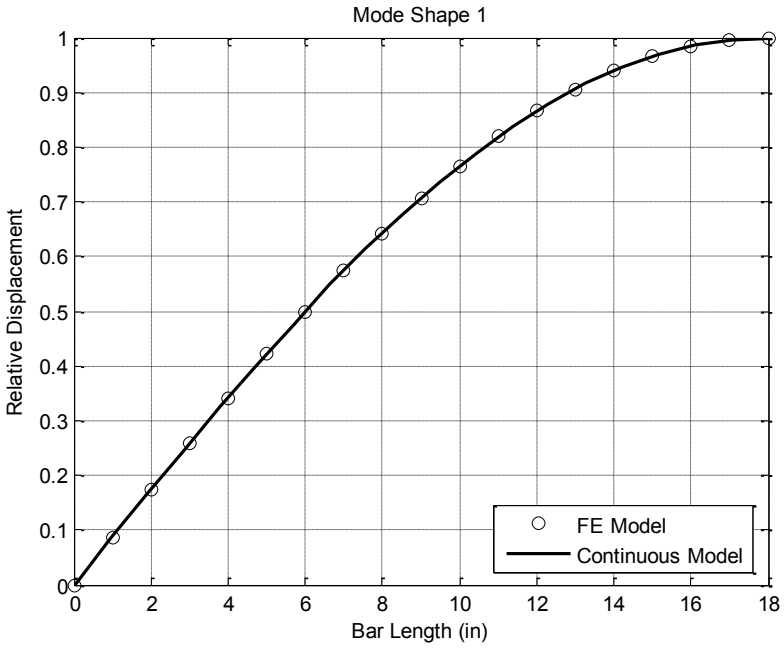

Figure 3.8: First Mode Shape of the Fixed Bar with Crack Depth of 0.01in.

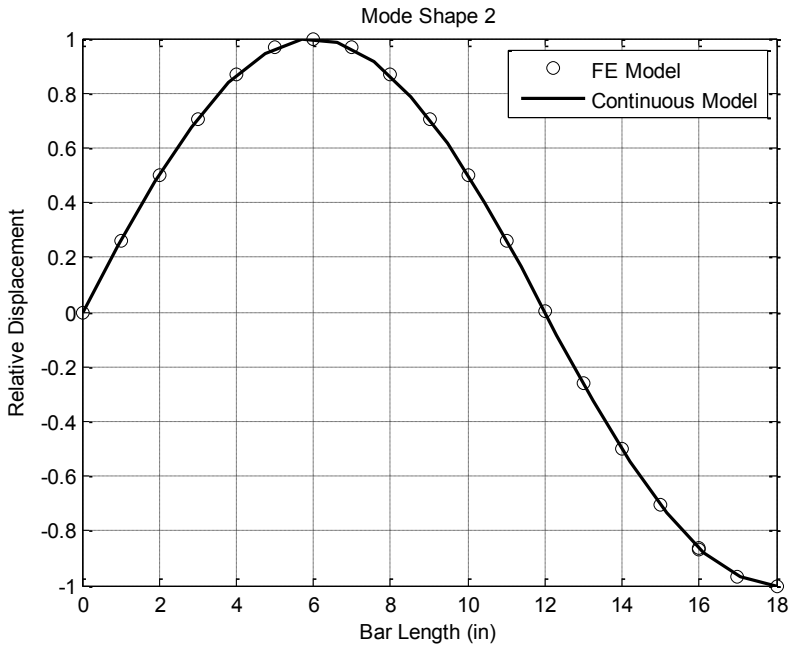

Figure 3.9: Second Mode Shape of the Fixed Bar with Crack Depth of 0.01in.

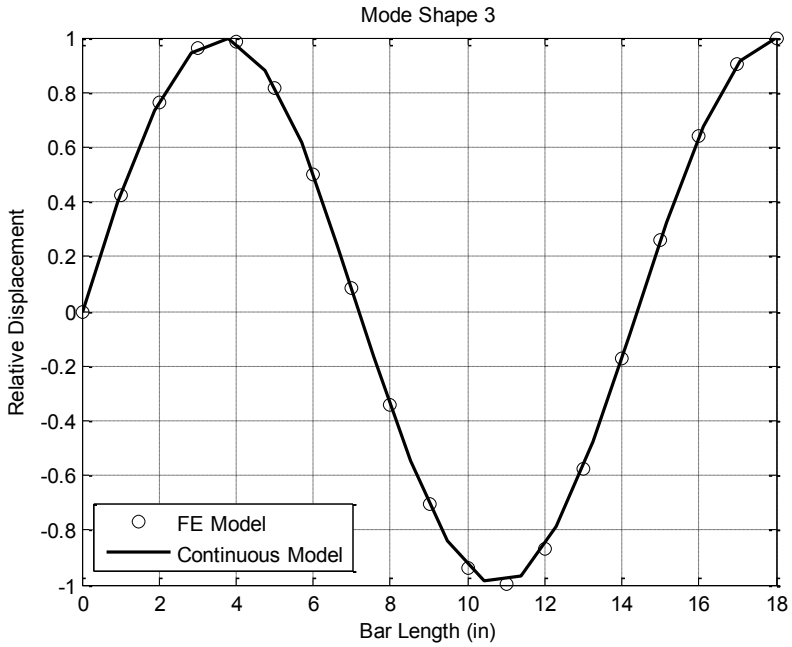

Figure 3.10: Third Mode Shape of the Fixed Bar with Crack Depth of 0.01in.

It can be clearly discerned that there is good agreement between the FE model and the continuous model. The results of the third natural frequency seem to diverge beyond 0.35in but this difference is insignificant. The first three natural modes obtained at a crack depth of 0.01in from the FE model also match very well with the results of the

continuous model. The third mode shape exhibits some difference between the two models, around 11in from the fixed end, but the mode shapes are very similar otherwise. Overall, the FE model effectively represents the actual model with minor differences that can be further reduced through modeling.

3.5.2. Example 2: Modeling of Triangular Truss-Comparison with ANSYS

Further validation of the FE model is performed by comparing the results with the results of commercial FE software, ANSYS. A triangular truss with an edge crack is used for this example. The objective of this example is to investigate the accuracy of the model for a triangular truss in comparison with the commercial FE software. The triangular truss used for this example is shown in Figure 3.5 with two members connected together through a pin joint in the form of an isosceles triangle. The left member, member 1, has a hinge support whereas member 2 is supported by a roller joint. The geometrical and material properties of the members are identical to those given to the bar in Example 1 except for the member length, which is kept as 9in for this example.

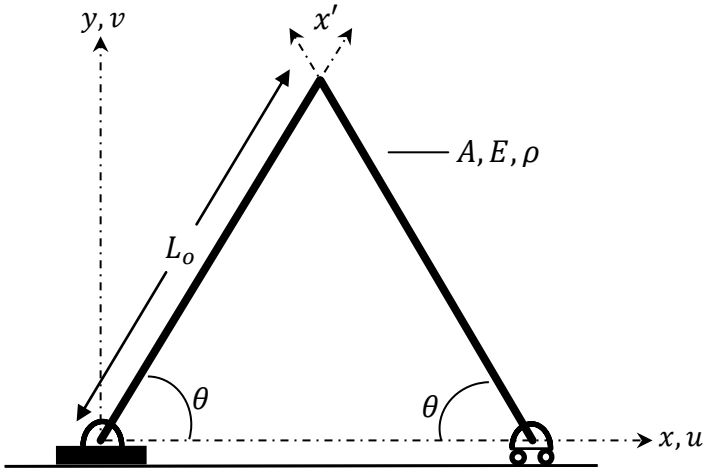

Figure 3.11: Triangular Truss with an Edge Crack.

The first three natural frequencies of the triangular truss are used to compare the results by varying four parameters: member angle θ, crack size a, crack location l_c, and number of elements el, per member. Summary of the results is tabulated in Table 3.1 for three different cases.

Table 3.1: Summary of First Three Natural Frequencies (Hz) of the Triangular Truss Modeled in MATLAB® and ANSYS.

	Case 1:	MATLAB	ANSYS	Case 2:	MATLAB	ANSYS	Case 3:	MATLAB	ANSYS
ω_1	$\theta = 0^o$	4921	4951	$\theta = 15^o$	3610	3165	$\theta = 60^o$	690	692
ω_2	$a = 0.2"$ $l_c = 4.5"$	11282	10866	$a = 0.2"$ $l_c = 4.5"$	5170	5190	$a = 0.45"$ $l_c = 4"$	5400	5340
ω_3	$el = 9$	14577	13754	$el = 21$	12910	12360	$el = 55$	12430	12416

In all cases of Table 3.1, the crack orientation β is set at 45° forming a mixed-mode crack with equal contribution of opening mode and shearing mode. The mixed-mode crack introduced in member 1 is located at 4.5in along the member length from the fixed joint. The maximum relative difference is found for ω_3 with about 6% in Case 1. It can be seen from Case 2 that increasing the number of elements for each member to 21 improves the accuracy. The crack size as well as the crack location is kept unchanged whereas the truss member angle is set at 15°. A major drop in ω_2 due the change in member angle is observed in Case 2 and an additional significant drop is recorded in Case 3 for ω_1. The relative difference of ω_1 in Case 3 is founded as small as 0.3%. A significant improvement in accuracy for ω_3 is observed by discretizing the member into smaller elements, resulting in a relative difference of 0.1%. Thus, it can be concluded that the FE model is capable of simulating more complex structures and is capable of providing accurate results even with a relatively coarse mesh. Furthermore, the results are comparable to the results of the commercial software, ANSYS.

3.5.3. Example 3: Application of Modal Analysis for Damage Detection

This example is continuation of Example 2 with the results obtained only from the FE model that has been developed in MATLAB®. This example is particularly used for studying various parameters and their influence on modal properties in order to investigate the viability of using modal analysis for damage detection. The parameters used as variables in this example are crack size, a, crack orientation, β, crack location, l_c, and truss member orientation, θ. These parameters are varied to study their influence on natural frequencies and mode shapes due to the presence of an edge crack in a member of the structure. The sensitivity of natural frequency to a change in the above listed variables is investigated. For a Mode-I crack introduced in the triangular truss with the member oriented at 30°, it can be observed from Figure 3.12 that the sensitivity of frequency to the damage parameters varies. The first three natural frequencies of the damaged truss are normalized by dividing each one by its corresponding undamaged natural frequency ω_n^*.

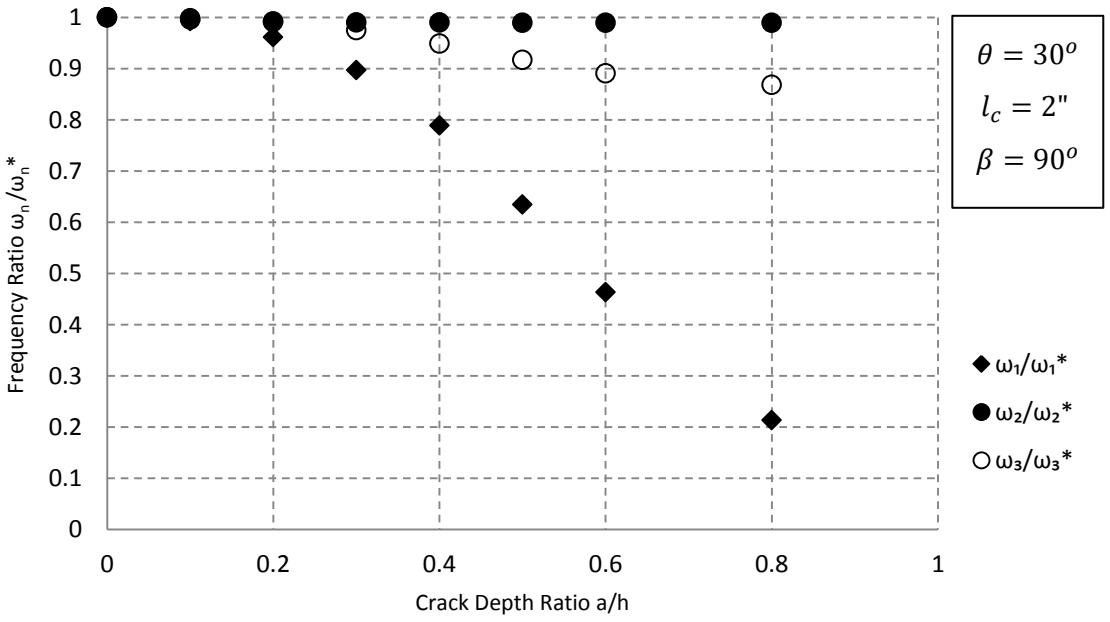

Figure 3.12: Frequency Ratio versus Crack Depth Ratio at Member Angle of 30°.

It may be noted from Figure 3.12 that changing crack depth ratio from zero to 0.8 shows that the first natural frequency has more than 80% reduction in frequency ratio, indicating high sensitivity to damage. On the other hand, the second natural frequency is least sensitive with a negligible change in frequency ratio. For a member angle of 45°, the value of the second frequency ratio holds at unity regardless of any change in the other parameters, as can be seen in Figure 3.13 and Figure 3.14. Therefore, it can be concluded the second frequency is expected to give a poor indication of damage. The second mode shape plotted in Figure 3.16, however, shows high sensitivity to damage in the global distortion scale due to the presence of a crack but a poor precision of crack location in detecting crack location. The other two mode-shapes in Figure 3.15 and 3.17 show lesser sensitivity to damage but demonstrate a much more accurate crack location for a crack depth of 0.2 or more.

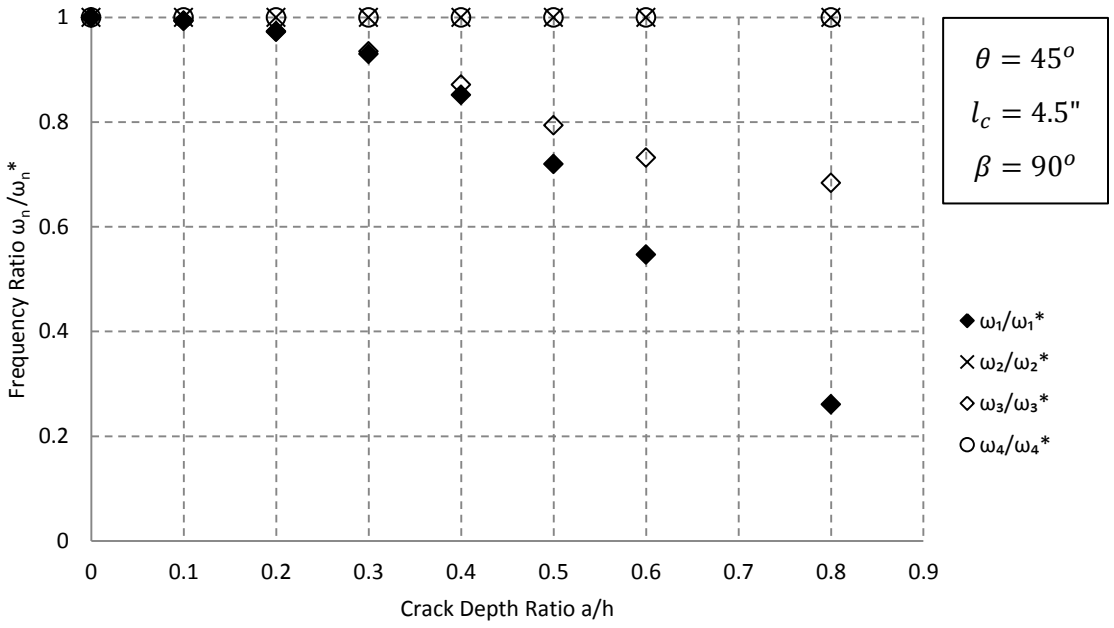

Figure 3.13: Frequency Ratio versus Crack Depth Ratio at Member Angle of 45°.

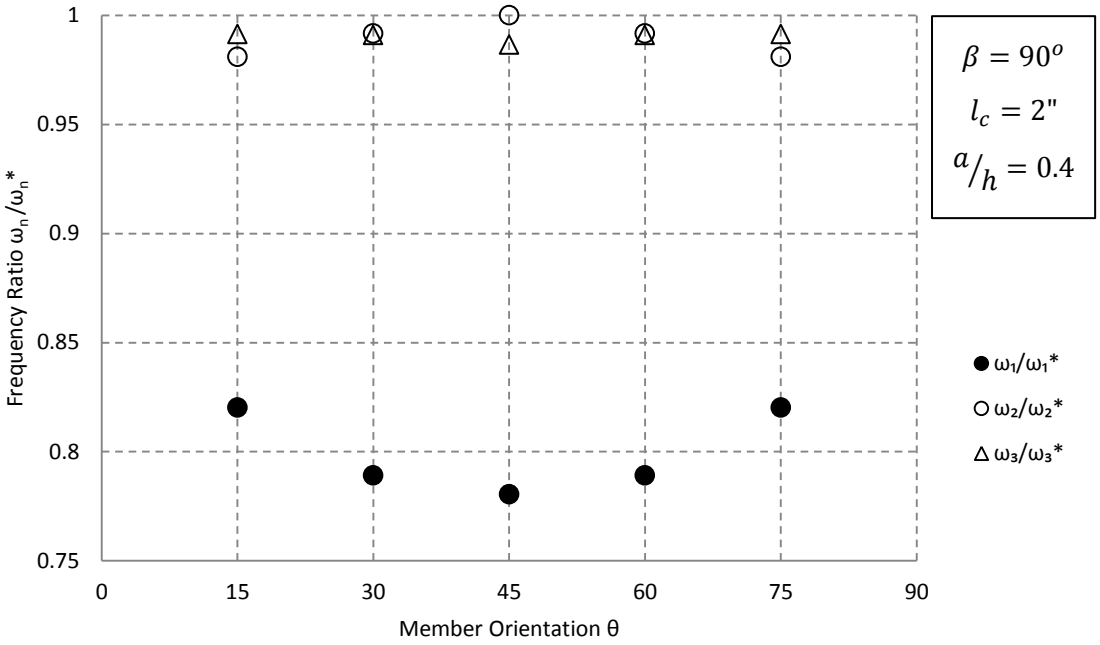

Figure 3.14: Frequency Ratio versus Member Orientation.

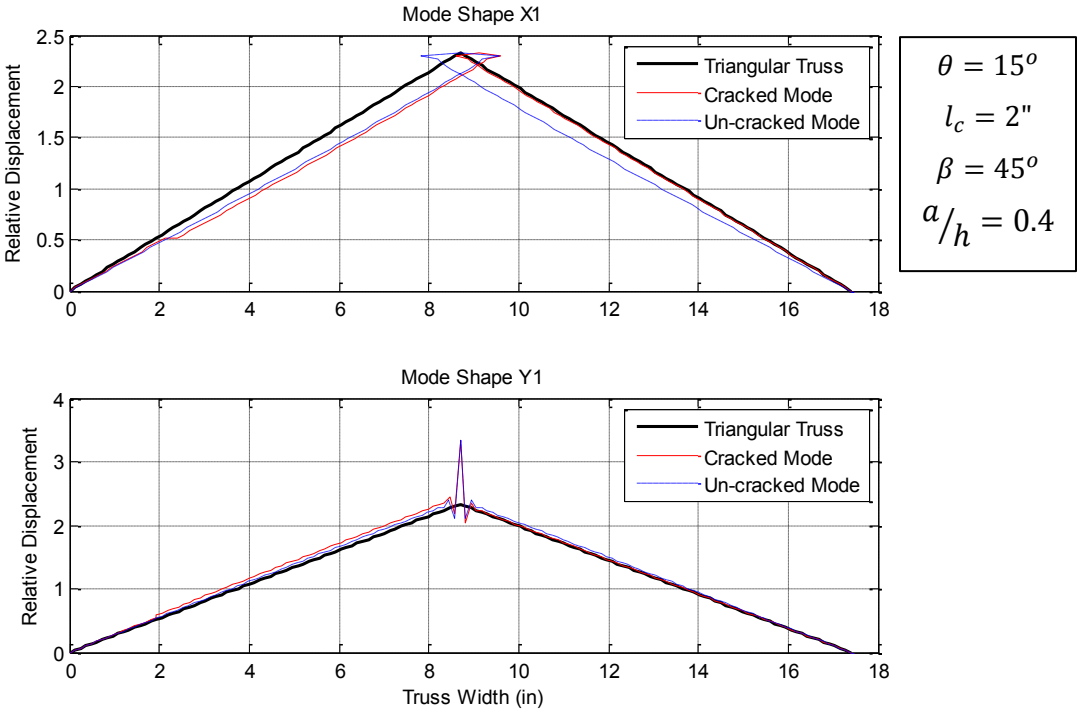

Figure 3.15: First Mode Shape of the Triangular Truss.

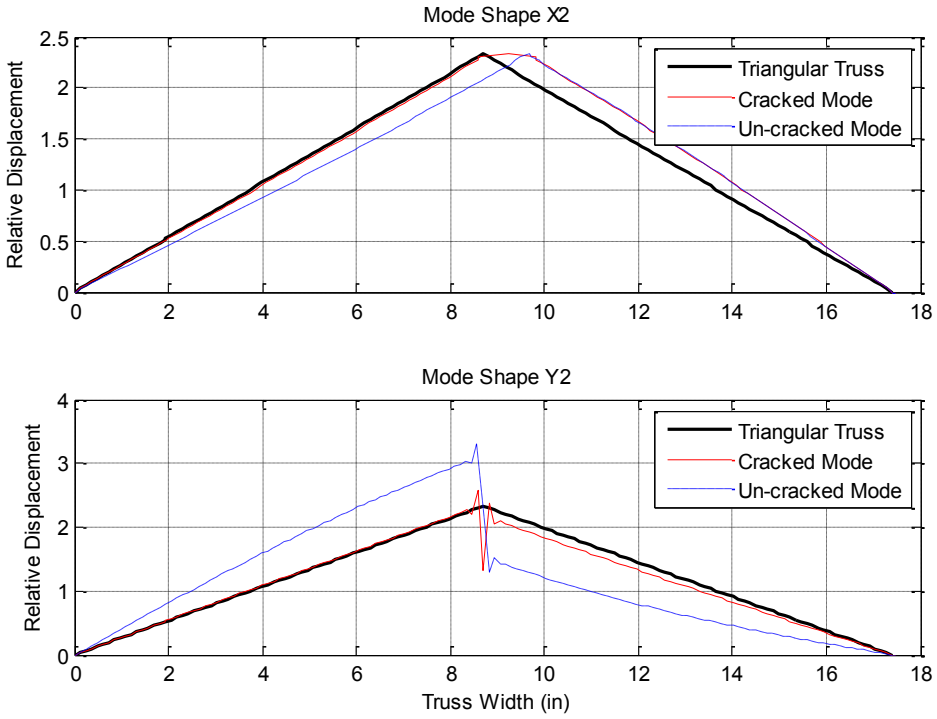

Figure 3.16: Second Mode Shape of the Triangular Truss.

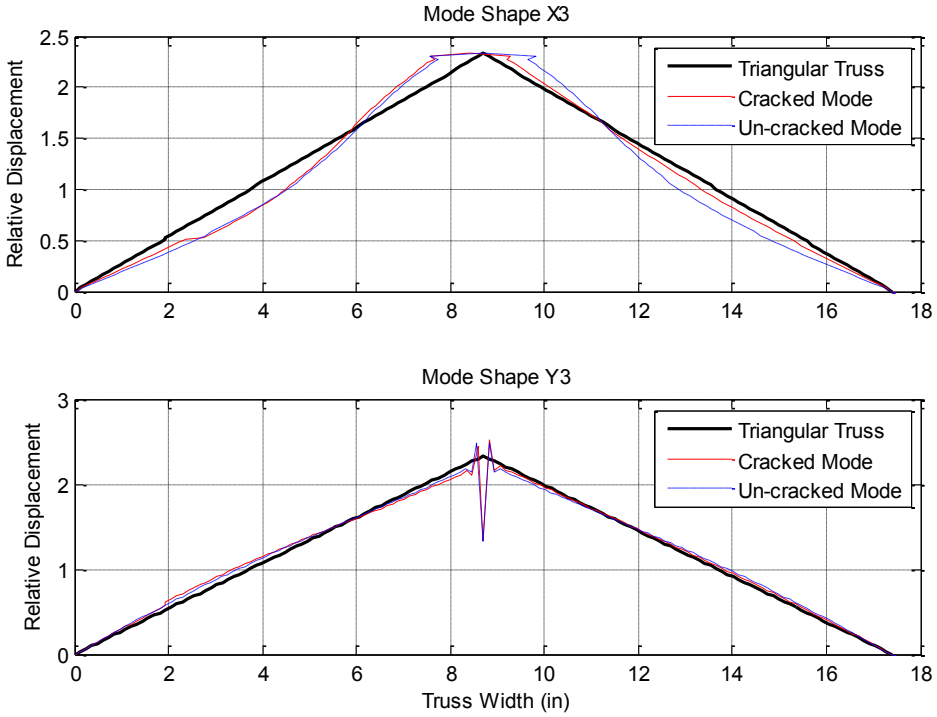

Figure 3.17: Third Mode Shape of the Triangular Truss.

As can be also observed from Figure 3.13, the even natural frequency ratios do not change significantly at member orientation of 45^o whereas the odd ratios can be seen to change. In a simpler structure like a bar, frequency ratio does not diverge from unity when the crack is located at the vibrational nodes [20] but in the triangular truss, the same behavior is observed regardless of crack location. Member orientation effects on frequency ratios are considered in Figure 3.14 by varying the angle between 15^o and 75^o and the results show 45^o to be a symmetry angle. Varying the crack orientation reveals significant changes in frequency as well. Figure 3.18 demonstrates similar trends to the one observed in Figure 3.12, as the crack orientation varies from the crack being a mixed-mode crack to a Mode-I crack. Therefore, it can be concluded that the pure Mode-I crack indicates a high frequency sensitivity in the first frequency ratio which may be used for damage detection, but this sensitivity is controlled by crack location as indicated by Figure 3.19.

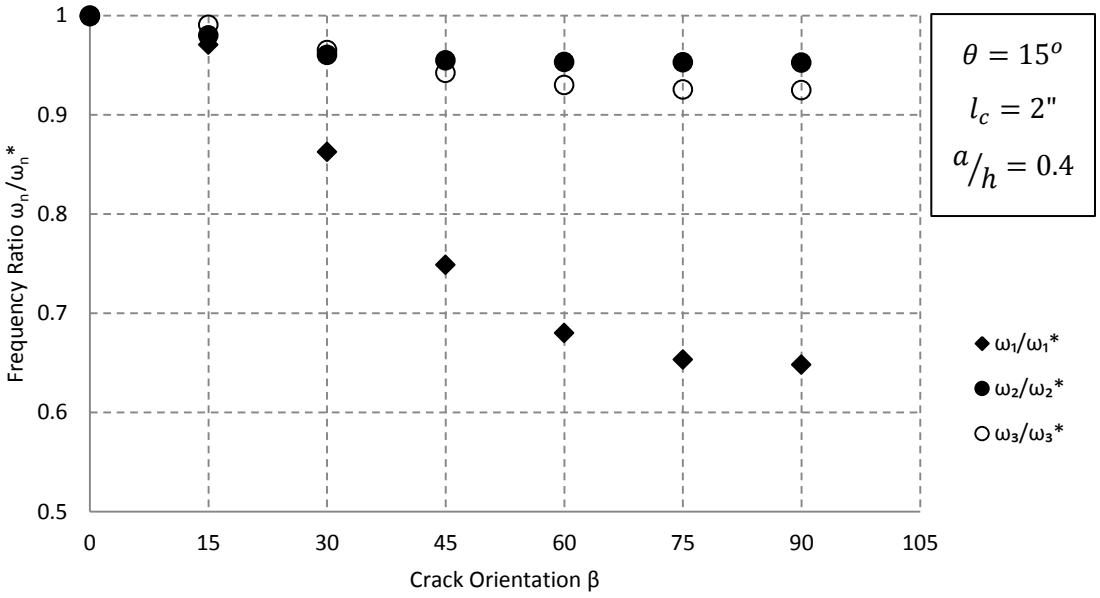

Figure 3.18: Frequency Ratio versus Crack Orientation.

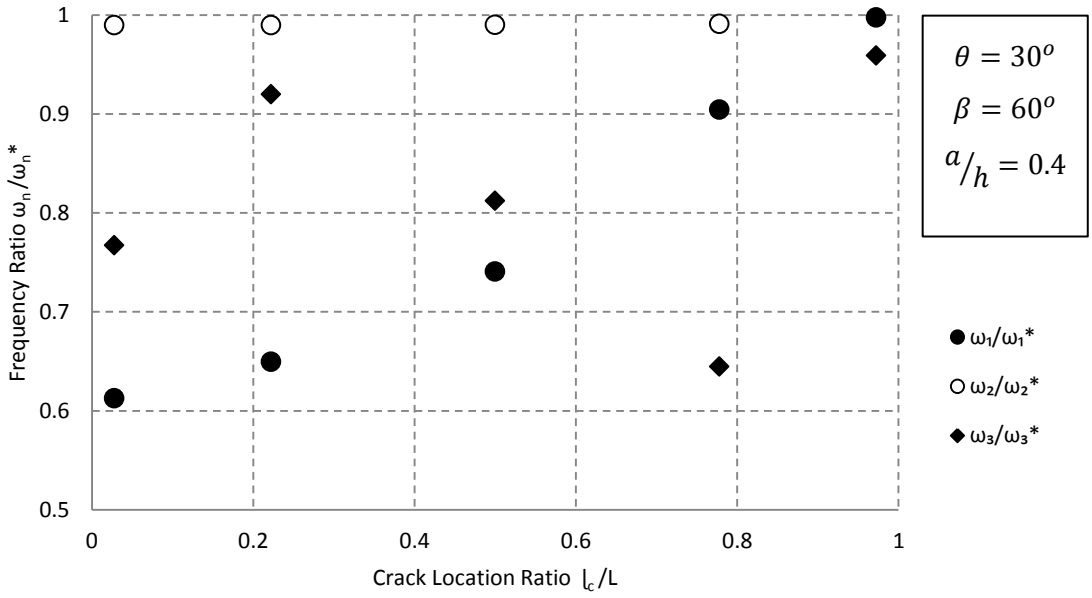

Figure 3.19: Frequency Ratio versus Relative Crack Location.

It may be noted from Figure 3.19 that the frequency sensitivity to the crack reduces until gets close to unity when the crack is located close to the connection joint. However, the third frequency shows a sinusoidal behavior as the crack location changes from the boundary to the connecting joint whereas the first frequency demonstrates a linear behavior. This implies that detecting damage that is close to the connecting joints in the truss may be much difficult to detect. As with all first three mode shapes discussed here for damage diagnostics, the crack introduced in a truss member has to be at least 40% of the member width and located within 20% of the member length from the joints so as to detect the presence of the damage. In addition, results of the mode shapes in Figures 3.15, 3.16, and 3.17 demonstrate the viability of using the traditional mode shape-based method for damage detection, revealing that this method also requires the natural mode shapes of the undamaged structure for comparison. These shortcomings of mode shape based method will be further discussed in Chapter 4.

3.6. Conclusions

The modal properties of a structural member of a truss as well as a triangular truss have been computed in this chapter. The fixed bar example demonstrates the capability of the FE model to accurately represent the cracked structural member with very high accuracy. The results obtained from the FE model and the continuous model provide an adequate confidence in the modeling approach. Furthermore, the FE model has been validated by modeling a simple triangular truss and by comparing the results to commercially available FE software. The results have further verified the viability of the FE model presented in this chapter. Modal analysis in the subsequent chapters will be continued with the FE model.

Application of the FE model integrated with a macroscopic model of a crack to accurately compute modal properties such as natural frequencies and mode shapes has been demonstrated and the viability of using modal properties for damage detection has also been investigated in this chapter. The sensitivity of natural frequency to damage is found to be primarily influenced by crack depth, crack location, and crack orientation but in some cases the natural frequency is found to be insensitive to damage. Thus, natural frequency may be a good measure of damage severity for relatively simpler structures, but cannot be used reliably for damage detection in complex structure. Likewise, mode shapes have the capability to detect and locate damage, but they seem to have limitations when the damage is located close to the boundary conditions (around 20% of the member length in the examples). Also the crack depth ratio needs to be relatively high (0.2 or more in the examples) in order for the mode shapes to detect damage. Using mode shapes to detect damage may require undamaged mode shapes especially when the mode shapes only show global distortion.

In the next chapter, Chapter 4, the wavelet transform will be used for extracting more information from the vibrational modes in order to identify damage characteristics. An algorithm for damage diagnostics will also be developed through the use of the wavelet transform to process the model response signal of a truss structure. The aim of using wavelet transform is to overcome the limitations of the traditional mode shape approach to a reasonable extent. Example 3 presented in this chapter will be revisited in Chapter 4 to quantitatively measure the performance of wavelet-based method in detecting and localizing damage using attributes of the modal response.

Chapter 4

Wavelet Transform and Damage Detection Algorithm

The wavelet transform is being increasingly used by researchers to identify signal irregularities or for detecting localized damage. The major advantage of the wavelet transform over the conventional methods such as the Fourier transform is that it provides time (space) resolution and scale (frequency) resolution, allowing it to perform local analysis for a given signal [38]. These characteristics enable the wavelet transform to describe local events in a signal and determine where (when) they occur, and making its use very attractive for damage detection methods [1]. In this study, a damage detection algorithm based on the Continuous Wavelet Transform (CWT) is developed to overcome the shortcomings of the mode shape-based method that has been discussed in Chapter 3. The algorithm has been specifically used in detecting mixed-mode cracks in truss structures. The proposed algorithm is a response-based damage detection method that requires a modal response signal from the fundamental mode shapes of a damaged structure to identify the damage location in the space domain. The spectral aspects of the wavelet transform and some commonly used wavelets are discussed in this chapter along with some of the properties associated with the application of wavelets. The process of selecting the appropriate wavelet is also discussed in this chapter by using several families of wavelets to detect damage in a simple truss structure. Commonly used filtering windows are also examined to evaluate the effective window for filtering any undesirable effects in the spatial wavelet transform. An outline of the damage detection algorithm is presented in this chapter, and the application of the algorithm is

tested through a numerical example by detecting and locating damage in a triangular truss structure.

4.1. Wavelet Transform and Wavelets

The wavelet transform is a unique signal processing technique that can be used in damage detection due to its ability to extract information about singularities from a signal or a function. An abrupt change in the wavelet coefficients indicates the presence and location of a defect, and the magnitude of local wavelet coefficients can also be correlated to damage severity. As discussed in the literature review presented in Chapter 2, it has been found that wavelets can be used as a filtering technique to de-noise data, and as a windowing transform to identify signal characteristics by using, what is called as, an analyzing wavelet. The CWT of a function, $f(x)$, with an independent space variable, x, is defined as [20, 29]:

$$C(u,s) = \frac{1}{\sqrt{s}} \int_{-\infty}^{\infty} f(x)\, \psi\left(\frac{x-u}{s}\right) dx \tag{4.1}$$

In Eq. (4.1), the CWT is stated as a convolution of the function, $f(x)$, and the analyzing wavelet, ψ, resulting in wavelet coefficients, $C(u,s)$. The function is decomposed by the mother wavelet, ψ, that is translated/shifted by a factor u, and dilated/scaled by a factor s. The scale factor is a positive quantity, controlling spatial resolution by stretching and compressing the wavelet. There are several families of wavelets with unique properties that can also influence damage detection such as number of vanishing moments, regularity, support, symmetry, etc. [38]. At a lower scale factor, the wavelet function has a smaller effective support, yielding a sharp spatial resolution that enhances identifying local events such as discontinuities [20, 30]. Similarly, the wavelet function with a higher scale factor is associated with a wider effective support, yielding a coarse spatial resolution that is better to identify long range events such as removed members [24]. This makes scale factor an important criterion in

the selection of the most appropriate wavelet for damage localization. To detect singularities in a signal, it is also important that the analyzing wavelet be sufficiently regular in order to avoid inconsistent regularity in the data which can yield incorrect results. The wavelet regularity is linked to the number of vanishing moments that controls the sharpness of the transition in wavelet coefficients and the magnitude of these coefficients near a singularity in the signal [29].

Some of the commonly used wavelet families such as Haar, Daubechies, Symlets, Coiflets, and Morlet are briefly discussed in this section. Haar wavelet is the simplest with no support and one vanishing moment, making it irregular and discontinuous at three points. The Haar wavelet can be explicitly expressed as [20]:

$$\psi(x) = \begin{cases} 1 & if \ \ 0 \leq x \leq \frac{1}{2} \\ -1 & if \ \frac{1}{2} \leq x \leq 1 \end{cases} \tag{4.2}$$

It can be noted from Eq. (4.2) that the Haar wavelet resembles a step function with a zero average in the space domain. Haar wavelet can also be constructed from the Daubechies wavelet family with $N = 1$ as the number of vanishing moments. Daubechies wavelets (db*N*) are asymmetric and have an arbitrary regularity, with higher regularity at some points. Symlets (Sym*N*) can be considered as an updated version of the Daubechies family, and both families have an identical number of vanishing moments. However, Symlets are nearly symmetrical with an arbitrary number of vanishing moments. Coiflets (Coif*N*) have similar properties to those of the Daubechies wavelets and Symlets, and are used in similar applications, but the number of vanishing moments is lesser by a quantity of one [39]. Morlets (Morl) do not have a scaling function or any vanishing moments, and can only be used in a CWT. However, Morlets are infinitely regular and symmetric with a signal effective support from -4 to $+4$. A common form of a Morlet wavelet is expressed as:

$$\psi(x) = Ce^{-x^2/2}\cos(5x) \tag{4.3}$$

In Eq. (4.3), C is the normalization constant.

This section provides a brief overview of some of the commonly used wavelets. A comprehensive discussion of wavelets and their properties as well as potential applications can be found in the literature [39]. The wavelets introduced in this section will be investigated in Section 4.4 through numerical examples in order to choose the wavelet that is best-suited for this study.

4.2. Filtering Windows

As discussed in Section 4.1, wavelet analysis can also be used to de-noise a signal, but using wavelets often results in some side peaks in the spatial domain that need to be sufficiently attenuated, especially for a low scale factor. Using a filter window is a common method to enhance the singularity resolution and to minimize the magnitude of the undesirable peaks. Several windows such as rectangular, triangular, Hanning, Hamming, Blackman, Kaiser, etc. have been used in the existing literature [40]. The selection of an appropriate window is a crucial step that could play an important role in the quality of overall results. Mathematically, filtering is defined as follows [41]:

$$H_L(n) = w(n)C(n) \tag{4.4}$$

In Eq. (4.4), $H_L(n)$ is the windowed signal, l is the length of the window, n is the number of sampling points, $w(n)$ is the filtering window, and $C(n)$ is the set of wavelet coefficients. A rectangular window is the simplest option and can be represented as a step function with a fixed amplitude value of one. A triangular window is similar to a Bartlett window and sharply reduces the magnitude of wavelet coefficients to zero at the ends while exercising no influence on the singularity of the function [40]. A Hanning window is widely used due to its ability to provide a sharp spatial resolution while

minimizing the amplitude of side peaks to a reasonable signal-to-noise ratio (SNR). The SNR is defined in decibels using the amplitude ratios as:

$$SNR_{dB} = 10\log_{10}\left(\frac{A_{signal}}{A_{noise}}\right)^2 \tag{4.5}$$

The symmetric expression of the Hanning window can be defined as follows:

$$w(n) = 0.5 - 0.5\cos\left(\frac{2\pi n}{l-1}\right), \qquad 0 \le n \le M-1 \tag{4.6}$$

In Eq. (4.6), M is $l/2$ for even values of l, and $(l+1)/2$ for odd values of l. The Hamming window is very similar to the Hanning window but it doesn't drop off to zero, resulting in the side peaks to be partially attenuated. The spectral aspect of the Hamming window can be defined as:

$$w(n) = 0.54 - 0.46\cos\left(\frac{2\pi n}{l-1}\right), \qquad 0 \le n \le M-1 \tag{4.7}$$

Another window that is commonly used for filtering purposes is known as the Blackman window. This function is able to minimize the side peaks even further with a smaller width of the main peak with a higher decay rate. The Blackman function can be expressed as follows:

$$w(n) = 0.42 - 0.5\cos\left(\frac{2\pi n}{l-1}\right) + 0.08\cos\left(\frac{2\pi n}{l-1}\right), \qquad 0 \le n \le M-1 \tag{4.8}$$

It may be noted from Eq. (4.8) that this window cuts off to zero at the ends of the spatial domain, resulting in a significant reduction of the side peaks. As with the use of the Kaiser window that has a controllable parameter for the side peaks, all the windows discussed here can be approximately produced. The following expression defines the Kaiser window [41]:

$$w(n) = \frac{I_o\left(\beta_k\sqrt{1-\frac{4n^2}{(l-1)^2}}\right)}{I_o(\beta_k)}, \qquad -\frac{(l-1)}{2} \le n \le \frac{(l-1)}{2} \tag{4.9}$$

In Eq. (4.9), $I_o(.)$ is the modified 0^{th} order Bessel function of the first kind, and β_k is the attenuation parameter. The Kaiser window is unique since it uses an attenuation parameter that is able to control the decay rate as well as the magnitude of the side peaks.

4.3. Damage Detection Algorithm

The primary concept of the algorithm developed in this study for detecting damage depends on localizing the maximum absolute value of wavelet coefficients from the modal response of a damaged structure. The selection of the appropriate wavelet and the filtering window depends on the application, and is usually done iteratively. Prior knowledge can be used to nominate candidates to expedite the process of selection. To localize damage from the modal response of a structure, the chosen wavelet should be sufficiently smooth and regular in order to avoid multiple discontinuities that may lead to incorrect results. Haar wavelets can be discarded since they are discontinuous and irregular. Another essential property in wavelets that enhances the reliability of damage localization is symmetry. Daubechies wavelets are asymmetrical and fairly regular if the number of vanishing moments is large enough, but coarse spatial resolution (space/time resolution) is inherently associated with a large number of vanishing moments [39]. Morlets are symmetrical and have infinite regularity, but require a higher number of sampling points for better representation of spatial resolution than Coiflets and Symlets [39]. As with all wavelets, the number of sampling points required to represent the shape of a wavelet is an important parameter that controls the spatial resolution, especially with a coarse sampling. From a practical viewpoint, the higher the number of sampling points, the higher the computational cost associated with implementing the technique on a real structure. Thus, it would be preferable to develop an algorithm with a wavelet that can accommodate coarse sampling, and at the same time is able to identify and locate the

damage reasonably well. Symlets and Coiflets are commonly used in some applications that are similar to damage detection. Therefore, these two families of wavelets as well as Morlets will be utilized in the simulations in Section 4.4 to judiciously select a suitable wavelet, as well as the associated parameters for the development of the damage detection algorithm.

From the discussion of the filtering windows in Section 4.2, it can be concluded that the selected filtering window should be able to significantly reduce the magnitude of side peaks without compromising the spatial resolution. There is a tradeoff between reducing the side peaks and the resolution of the main peak that is caused by a discontinuity resulting from damage. Using the triangular window reduces the amplitude of wavelet coefficients linearly, yielding a long range of coefficients that are significantly reduced and consequently a larger infeasible region. Similarly, the Hamming window also is not expected to be an appropriate choice for the analysis. The Kaiser window is the most appropriate for the application investigated in this study since it increases the SNR and does not cut off to zero sharply. Furthermore, an attenuation parameter, β_k, can be used to control the side effects more effectively. Numerical examples to justify the selection of the filtering window to enhance the spatial resolution will be presented in the next section.

Some statistical measures are incorporated in the development of the algorithm in order to remove the outlier data points from the results. The mean and standard deviation of the damage location, l_c, are calculated as follows:

$$\sigma_c = \sqrt{\frac{1}{n}\sum_{i=1}^{n}\left(l_{c,i} - \overline{l_c}\right)^2}\ , where\ \ \overline{l_c} = \frac{1}{n}\sum_{i=1}^{n} l_{c,i} \tag{4.10}$$

In Eq. (4.10), n is the number of data points, $\overline{l_c}$ is the mean of the calculated damage location, and σ_c is the standard deviation of the damage location. The outlier

data points that are within a specific value of standard deviation (α) from the mean are removed from the set of the data points so as to recalculate the updated mean of the damage location. The value of α will be determined from the simulation analysis conducted in Section 4.4. After calculating the updated mean, the normalized error of the results can be determined as follows:

$$Error = \left|\frac{\bar{l_c} - l_a}{l_m}\right| 100\% \tag{4.11}$$

In Eq. (4.11), l_a is the actual damage location and l_m is the length of the member. Calculating the error allows an evaluation of the robustness of the proposed algorithm to detect and locate damage. The following steps outline the proposed damage detection algorithm.

1. Obtain the first three mode shapes, X_i, of a damaged truss structure, and extract the first three mode shapes of each member, $X_i^{(m)}$, in the global coordinate system, $X_{ix}^{(m)}$ and $X_{iy}^{(m)}$.
2. Using the mode shapes of each member, compute the continuous wavelet coefficients and apply a filtering window to the data using the most appropriate wavelet and the filtering window. The filtering window will be selected in the subsequent section.
3. Localize the maximum absolute value of wavelet coefficients along with their location, l_c, within the length of a damaged member for each mode.
4. Perform the statistical analysis for the data from Step 3 and remove the outlier data points that are beyond α standard deviations of the mean, and then recalculate the mean of the updated set of damage location.
5. Report damage location within the member length and the normalized error associated with the predicted damage location.

6. Plot wavelet coefficients versus member length for the mode shapes that are required to locate the damage.

This algorithm is finalized with the selection of an appropriate wavelet along with its associated parameters and a filtering window to efficiently reduce the side peaks while preserving a sharp spatial resolution. Moreover, identifying the outliers with the use of the statistical analysis requires finding a value of α to locate the damage with a reasonably small error. All these parameters are determined in the next section.

4.4. Application of The Algorithm – Triangular Truss

The triangular truss structure that has been discussed in Section 3.4 is revisited here to finalize some of the parameters associated with the algorithm, and to evaluate the capability of the algorithm. Some related characteristic aspects of the triangular truss that were presented in Section 3.4.2 are presented again for the sake of completeness. The triangular truss has two members, namely 1 and 2, each with a length of 9in and the members have identical material and geometrical properties that have been provided in Section 3.4.2. A mixed-mode crack with a crack size of 0.07in and crack orientation of 45^o is introduced in member 1 at 2in along the member length from the fixed joint. The triangular truss is oriented at 60^o.

In Table 4.1, a list of wavelets used to obtain wavelet coefficients from the CWT are provided along with the number of vanishing moments (if applicable) that are found to give a reasonable spatial resolution with lower sensitivity to noise. The wavelet results are filtered through the Hanning window to minimize edge effects caused from the use of the wavelet transform. The predicted damage location of mode shape 1 as well as the mean of the damage location, $\overline{l_c}$, through the use of the first three natural mode shapes is also reported in Table 4.1 by locating the absolute maximum wavelet coefficients along the member length. The wavelet results of the first mode shape are used to select

a suitable wavelet that can efficiently detect the damage with lower edge effects since this mode was found to have lower sensitivity to damage than the higher modes as shown in Chapter 3. The normalized error associated with the updated mean of the predicted damage location is also presented in Table 4.1 to investigate the capability of each wavelet in locating the structural damage.

Table 4.1: Results of Triangular Truss with a Damaged Member.

Wavelet	Vanishing moments, N	Predicted location, (in), l_c			Error %
		x1	y1	$\overline{l_c}$	
Symlet	4	2.000	2.000	2.000	0.0
Coiflet	2	2.250	2.250	2.250	2.8
Morlet	---	2.375	8.625	2.375	4.2
Daubechies	3	2.250	2.250	2.250	2.8

It can be seen from Table 4.1 that the number of vanishing moments is different for each wavelet, this has been determined iteratively so that the wavelet has sufficient regularity and little sensitivity to noise. For all the wavelets listed in Table 4.1, the scale factor that ensures the accuracy of damage localization while maintaining a sharp spatial resolution is found to be 2 as can also be seen in Figure 4.1. The results show that the proposed algorithm is able to detect the singularity caused by a crack by using Sym4 (from the Symlet family), exactly at the predefined crack location. In contrast, using Coif2 or db3 locates the crack within 2.8% of the actual crack location from all three mode shapes. It can be observed from Table 4.1 that using Morlet to process the mode shapes requires removing the data point obtained from the first natural mode shape in the y-global coordinate system because it is an outlier. Thus the updated mean of the crack location is computed as 2.375in with an error of 4.2%.

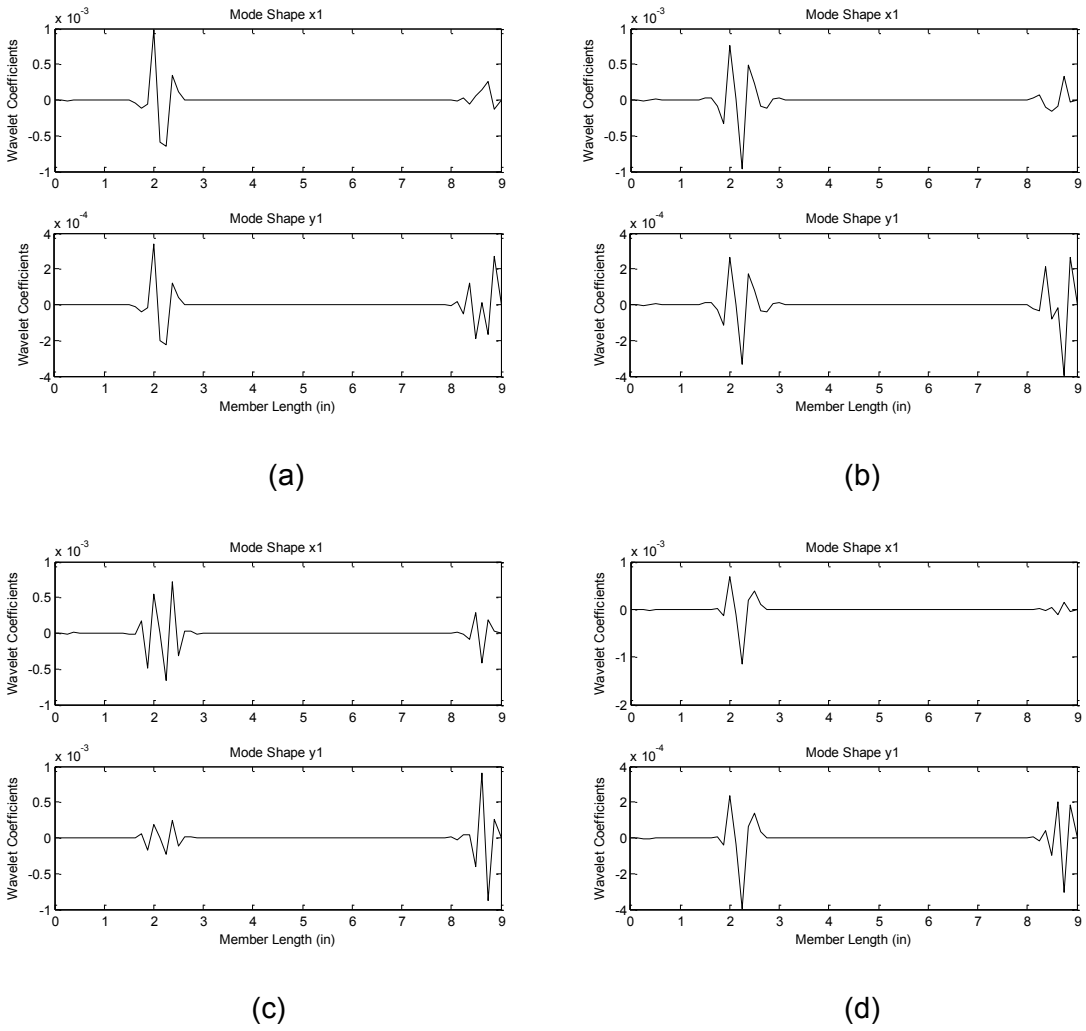

Figure 4.1: Wavelet Coefficients of Mode Shape 1 Using Four Wavelets: (a) Sym4, (b) Coif2, (c) Morl, and (d) Db3.

The wavelet results presented in Table 4.1 are plotted in Figure 4.1 using wavelet coefficients versus member length to extract additional information regarding the characteristics of the analyzing wavelets. It can be discerned from all the plots that the end effects are clearly apparent on the right side of the spatial domain, and this could be attributed to the fact that the end effects caused by the free joint are much higher than those caused by the fixed joint. Furthermore, these end effects indicate that the Hanning window does not sufficiently mitigate noise. It can be concluded that the most appropriate wavelet for this application is Sym4, and assigning value of 1 for α has been found to successfully identify the outlier data points.

The filtering window has been set as a variable in Table 4.2 while analyzing the chosen wavelet, Sym4, with the value of α kept constant for this analysis. The wavelet results are filtered using five windows including the triangular window that has been reviewed for completeness. Table 4.2 shows damage location results from the evaluation of the first vibrational mode with the overall updated mean damage location and the error associated with the results. Another parameter has been added to Table 4.2 in order to select the appropriate filtering window, this is the SNR which is computed for each window from the amplitude of wavelet coefficients at the main peak and the side peaks.

Table 4.2: Results of Triangular Truss with a Damaged Member, Five Windowing Functions.

Window	SNR_{dB}	Predicted location, (in), l_c			Error %
		x1	y1	$\overline{l_c}$	
Triangular	-32.943	8.625	8.750	8.750	75.0
Hanning	1.946	2.000	2.000	2.000	0.0
Hamming	-13.682	8.875	9.000	8.938	77.1
Blackman	6.700	2.000	2.000	2.000	0.0
Kaiser[20]	44.605	2.250	2.250	2.250	2.8

As expected, the results in Table 4.2 demonstrate that the triangular window and the Hamming window are poor choices for this application since they result in a high error and are more susceptible to noise, as can be seen in Figure 4.2a and b. It may be noted from Table 4.2 that the Hanning window and the Blackman window are able to localize the damage exactly at the predefined crack location, but cannot minimize edge effects as can be observed from the SNR values and the results in Figure 4.1a and Figure 4.2c. The Kaiser window with an attenuation parameter of 20 has the ability to reduce edge effects significantly, as seen by the SNR of 44.6 dB. However, this comes at the expense of increased error in determining the location of damage. The wavelet results of the Kaiser window in Figure 4.2d show a sharp spatial resolution of the first mode and a

small error in the predicted damage location. Therefore, this filtering window has been selected for the damage detection algorithm.

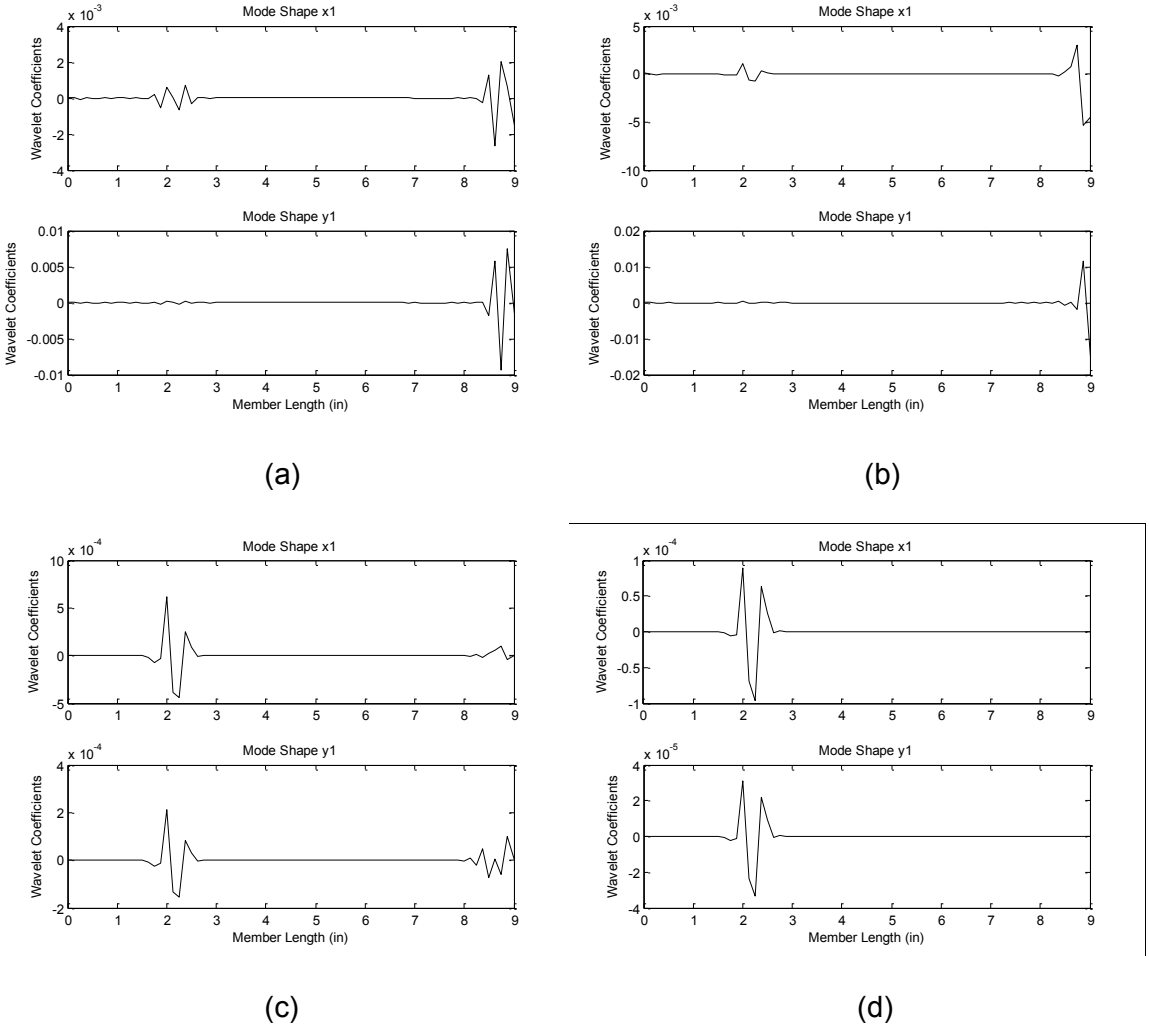

Figure 4.2: Wavelet Coefficients of Mode Shape 1 Filtered by Using Four Windows: (a) Triangular, (b) Hamming, (c) Blackman, and (d) Kaiser[20].

From the results discussed in this chapter, the use of the wavelet transform is found to be capable of identifying a crack as small as 0.07in precisely with the use of the first three mode shapes. This is an improvement over the mode shape-based method that has been discussed in Chapter 3, requiring the modal response of undamaged and damaged triangular truss structures to detect a crack that is at least 0.2in long. Furthermore, it has been observed that cracks located within around 20% of member

length from the joints are difficult to detect with the traditional mode shape approach. This limitation of the traditional approach can be overcome to a satisfactory extent by processing the mode shapes through the use of the wavelet transform. Table 4.3 investigates the feasible region by introducing a crack at four different locations along member 1. The mean of the damage location before removing the outliers,$\overline{l_{c,b}}$, and after removing the outliers, $\overline{l_{c,b}}$, is also provided to evaluate the reliability of the approach, as can be seen from the error.

Table 4.3: Results of Triangular Truss with a Damaged Member, Four Damage Cases (Crack Size: 0.07in).

Case #	Actual location, (in), l_a	Predicted location, (in), $\overline{l_c}$		Error %
		$\overline{l_{c,b}}$	$\overline{l_{c,a}}$	
1	1.0	1.25	1.25	2.8
2	2.0	2.25	2.25	2.8
3	4.5	4.50	4.50	0.0
4	8.5	7.53	8.53	0.3

The results of Table 4.3 demonstrate the ability of the algorithm to detect a small crack with varying crack locations with an error of less than 3.0%. In the first three cases from Table 4.3, the mean of data points before and after removing the outliers is identical because the standard deviation of the data is zero at these locations, but the error associated with cracks located closer to the joint is higher than the error calculated for the crack inflicted at the center of the member length. It can be concluded that the algorithm gives consistent and reliable results if the crack in the triangular truss is reasonably beyond the joints, by around 5% of the member length. This will be investigated further through other examples in the subsequent chapter.

4.5. Conclusions

The damage detection algorithm has been developed, and the associated parameters have been finalized for damage diagnostics in this chapter. Results from the use of several wavelets have been investigated by using the first three mode shapes of a damaged triangular truss. The most appropriate wavelet that provides a sharp spatial resolution and low edge effects is the Symlet (Sym4) with a scale factor of 2, and with 4 vanishing moments. Sym4 is found to be capable of efficiently correlating the wavelet coefficients to local damage characteristics. Additionally, multiple windows have been investigated for filtering the data obtained from Sym4. The Kaiser window with an attenuation parameter of 20 has been found to significantly reduce undesirable edge effects without excessively compromising the feasible region.

The results of the algorithm indicate that using the wavelet transform for damage diagnostics is viable and reasonably accurate. Furthermore, the application of the detection algorithm on a triangular truss structure using multiple damage cases shows that the wavelet transform can overcome the shortcomings of the traditional mode shape approach in detecting damage more precisely, and over a larger feasible region with relatively smaller error. The algorithm developed in this chapter will be tested in Chapter 5 by using larger and more complex truss structures so as to evaluate its robustness and reliability for detecting damage caused by mixed-mode cracks.

Chapter 5

Application of Damage Detection Algorithm to Large Truss Structures

This chapter examines the ability of the damage detection algorithm that has been presented in Chapter 4. The algorithm is used to detect mixed-mode cracks in truss structures in several numerical examples. The Warren truss and the Howe truss have been used for analysis. The damage is simulated by using the macroscopic model that is combined with the FE model, as discussed in Chapter 3. The modal response of the damaged structure is used to obtain the first three natural frequencies along with their corresponding mode shapes. The modal response is used to detect and locate damage, and evaluate damage severity. Wavelet results of the natural modes are also plotted for some cases in order to discuss the influence of varying parameters.

Multiple parameters associated with structural geometry and damage characteristics are used to comprehend the influence of these parameters on the performance of the proposed algorithm. The specific parameters that have been investigated in this study are as follows: number of truss members, location of damaged members within the structure, truss member orientation (geometry of the truss structure), crack size, crack orientation, and crack location (within member length). A crack size of 0.07in has been used for all the simulations in this chapter, and damage is introduced in one member at a time. Symlets (Sym4) with a scale factor of 2 have been used to generate the wavelet coefficients of the modal response. Normal distribution is assumed and data within one standard deviation of the mean are used for analysis.

The truss member orientation,θ, has been varied between 15^o and 60^o and the crack orientation,β, is changed such that the crack varies from a mixed-mode crack to a

purely Mode-I crack with β = 90°. The crack is predefined at a specific location, l_a, and is located along the length of the member as an edge-crack. The algorithm predicts the location of the damage, l_c, based on statistical measures and the predicted location is expressed in the local coordinate system of the damaged member, by setting the origin at the left joint of each truss member. The specific mode shapes that are used to predict the damage location are listed and the most sensitive natural frequency among the first three frequencies is also listed (identified as ω_n'), which is the ratio between the natural frequency of the damaged truss and the natural frequency of the undamaged truss. The normalized percentage difference, $E\%$, between actual crack location and predicted crack location is also calculated.

5.1. Warren Truss Structures

This section presents simulation results from the FE model as well as the results from the detection algorithm for the Warren truss structures. Figure 5.1 shows two Warren truss structures with 11 members and 23 members respectively, these truss structures have been used for analysis in this section. All the truss members shown in the two trusses in Figure 5.1 have identical geometry and material properties, as presented in Section 3.4.2. The members have a 0.021in × 0.5in rectangular cross section with a Young's modulus of 10.2Msi and a material density of 0.1lb/in^3. The length of each member located at the bottom and at the top of both structures is 9in. However, the length of the inclined members as well as the height of the structure is a function of the orientation,θ, a parameter that has been included in the analysis.

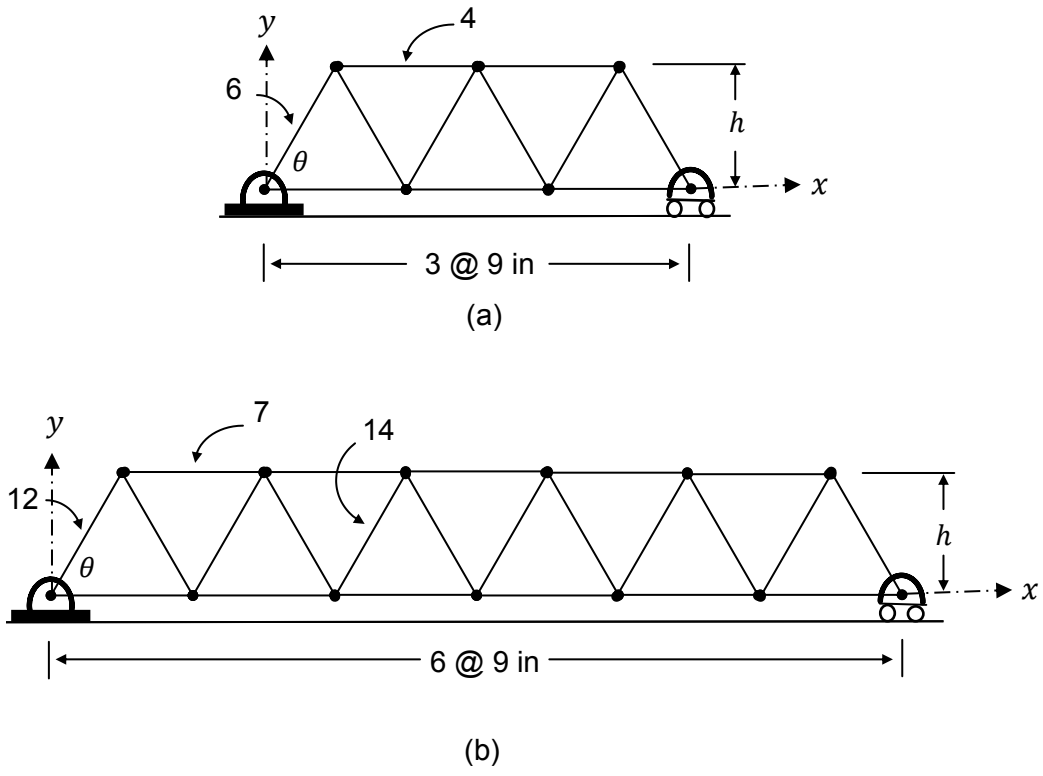

Figure 5.1: (a) Warren Truss – 11 Members with Two Damaged Members. (b) Warren Truss – 23 Members with Three Damaged Members.

5.1.1. Warren Truss – 11 Members

The Warren truss structure shown in Figure 5.1a consists of 11 members. The bottom members are identified from left to right as 1-3 and the top members are identified as 4 and 5. The numbering continues from left to right for the right-leaning members as 6-8, and the left-leaning members are numbered as 9-11. For this analysis, damage is introduced in two structural members, 4 and 6, as depicted in Figure 5.1a.

Multiple response characteristics of the damaged truss are captured by varying the model parameters. Eight cases for the damaged structure are discussed in order to examine the influence of each parameter on damage detection. In Table 5.1, the first four cases are associated with member 4 which is a horizontal member whereas the other cases are linked to member 6, an inclined member leaning to the right at an angle,

θ. Results from the damage detection algorithm for all the cases are presented in Table 5.1.

Table 5.1: Results of Warren Truss - 11 Members, Eight Cases with Two Damaged Members (Crack Size: 0.07in).

Warren Truss Parameters					Results			
Case #	Member ID	Member orientation (deg.), θ	Crack orientation (deg.), β	Actual location (in), l_a	Predicted location (in), l_c	Error %	Mode shapes	Natural frequency ratio, ω_n'
1	4	60	60	4.6	4.50	1.1	x1, x2,x3	ω_3, 0.995
2	4	15	60	4.6	4.50	1.1	x1, x2,x3	ω_3, 0.995
3	4	60	60	1.4	1.76	4.0	x1, x2,x3	ω_2, 0.995
4	4	60	45	7.6	7.43	1.9	x1, x2,x3	ω_3, 0.996
5	6	60	60	4.6	4.50	1.1	all	ω_3, 0.995
6	6	60	45	7.6	7.43	1.9	x2,y2,x3,y3	ω_2, 0.997
7	6	60	45	1.4	1.76	4.0	x2,y2,x3,y3	ω_3, 0.995
8	6	60	85	1.4	1.76	4.0	y1,x2,y2,x3,y3	ω_3, 0.994

In Case 1 in Table 5.1, a mixed-mode crack oriented at 60^o is located at 4.6in within the length of member 4 (measured from the left joint). As can be seen from the results in Table 5.1, the algorithm successfully predicts the damage location within 1.1% using the mode shapes in x-global coordinate. Mode shapes in the y coordinate are eliminated by the algorithm since these are considered as outliers. The presence of the crack does not exhibit any influence on the transverse direction because the horizontal (top and bottom) members are only oscillating longitudinally. Results of the wavelet transform corresponding to the mode shapes that are used to locate the damage are plotted as wavelet coefficients versus member length in Figures 5.2, 5.3, and 5.4. It can be clearly discerned from Figure 5.2 that a strong peak that is caused by the presence of a crack is associated with the highest amplitude coefficient of 0.0175 at 4.5in. Likewise, the highest peak is found at the same location in Figure 5.3 and Figure 5.4, but the amplitudes of the maximum coefficients in these figures are 0.045 and 0.09 respectively. It can be seen in

this case that higher modes are more sensitive to damage and provide a strong indication of the existence of damage. Natural frequency ratio corresponding to the third mode is found to be most sensitive with a value of 0.995. However, the change in the frequency ratio is very small and may not be detected in the presence of noise. It may be noted that the end effects caused by the connecting joints have been significantly reduced by filtering the data through a Kaiser Window. Also, the main peak caused by the discontinuity due to the presence of a crack is strengthened as the filter maximizes the ratio of the main peak energy to the side peak energy [42].

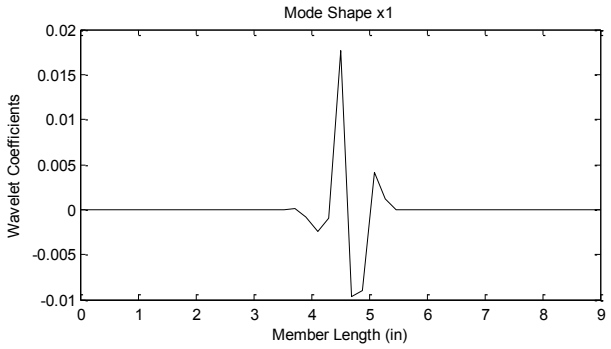

Figure 5.2: Wavelet coefficients of mode shape x1 (Case 1, Table 5.1).

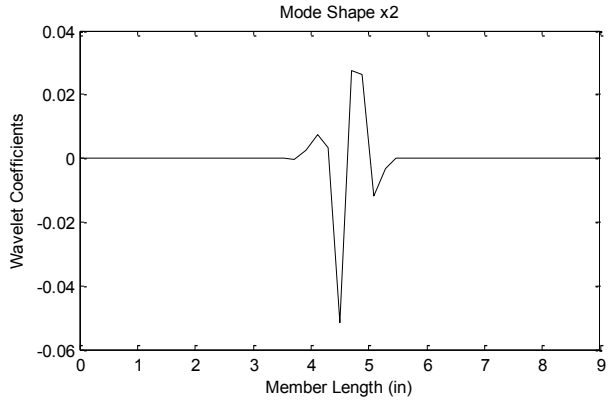

Figure 5.3: Wavelet Coefficients of Mode Shape x2 (Case 1, Table 5.1).

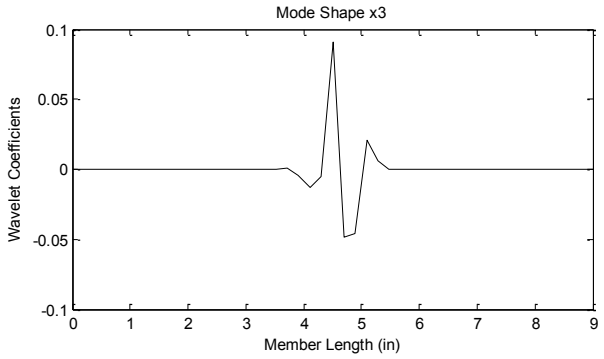

Figure 5.4: Wavelet Coefficients of Mode Shape x3 (Case 1, Table 5.1).

In Table 5.1, Case 5 demonstrates the influence of member location within the truss structure on the damage diagnostic technique. A crack is located at 4.6in in member 6 with the same characteristics as introduced in member 4 in Case 1. The truss member orientation is set at 60^{o}. As can be seen from Table 5.1, results for this case are identical to Case 1 except that additional mode shapes are required to locate the damage. Results of the wavelet transform for the three mode shapes (in global coordinates) are presented in Figures 5.5, 5.6, and 5.7. The results demonstrate a clear detection of discontinuity at the crack location. A trend is observed in the wavelet transform plots indicating that higher modes are associated with larger amplitudes of wavelet coefficients at the singularity. Likewise, the ratio of wavelet coefficients of mode shapes 2 and 3 to the wavelet coefficients of mode shape 1 are found to be relatively large. Wavelet results of all mode shapes in Case 5 show that the coefficients are smaller in magnitude at the crack singularity in the x-axis as compared to the y-axis. It can be seen from Figure 5.5 that mode shape x1 has a relatively smaller amplitude of wavelet coefficients as compared to mode shape y1. The end effects due to the joints are more apparent on the right side of mode shape x1 at 8in. This has also been observed in the triangular truss structure in Section 4.4. The underlying reason for this is that the geometry of the truss structure and the truss member orientation exercise an influence on the mode shape of the damaged structure. Truss member orientation in inclined

members controls the contribution on mode shapes in the global coordinates. Therefore, a member orientation of 60^o contributes more to the mode shape along the y-axis, whereas a member orientation of 45^o contributes equally in both directions of the global mode shapes. It is observed from the wavelet results of Case 1 and Case 5 that the damage introduced in the inclined members is significantly influenced by truss member orientation whereas the damage in the horizontal members shows little sensitivity to varying truss orientation.

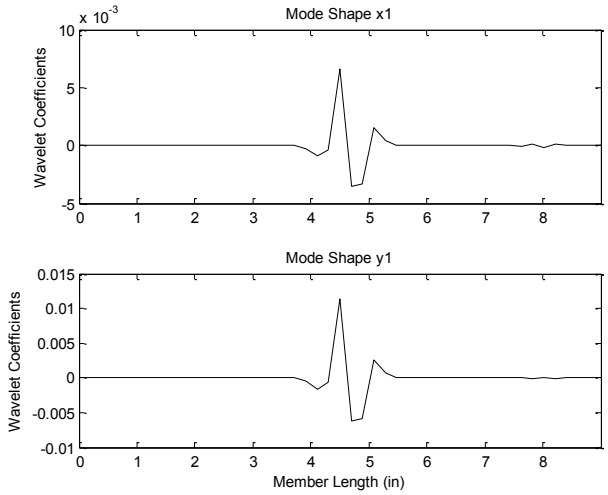

Figure 5.5: Wavelet Coefficients of Mode Shape 1 (Case 5, Table 5.1).

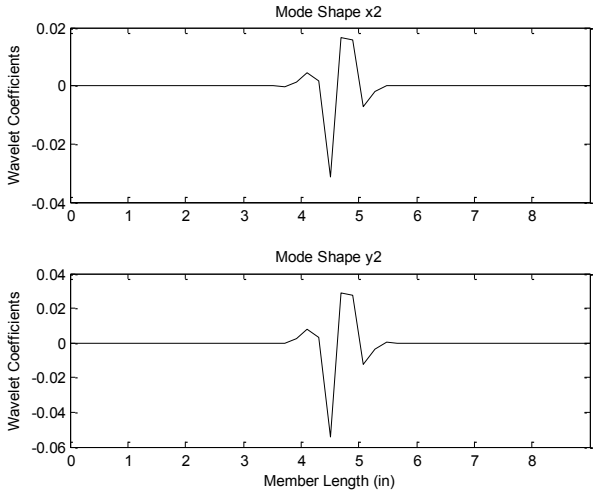

Figure 5.6: Wavelet Coefficients of Mode Shape 2 (Case 5, Table 5.1).

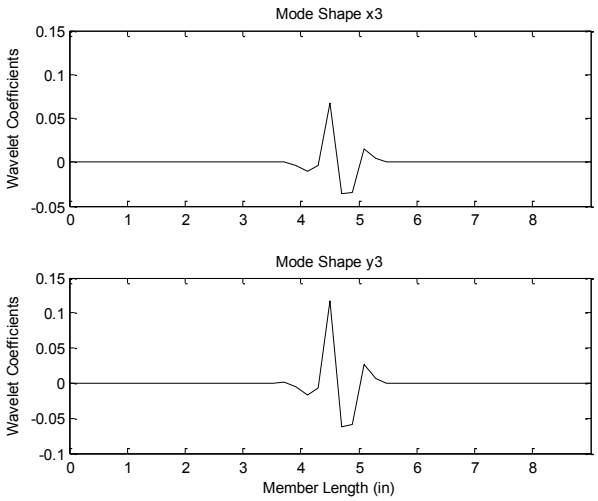

Figure 5.7: Wavelet Coefficients of Mode Shape 3 (Case 5, Table 5.1).

The influence of the crack orientation parameter on damage detection is demonstrated in Case 7 and Case 8 using a mixed-mode crack with an angle of 45^o and 85^o respectively. The crack is located at 1.4in on member 6 that is orientated at 60^o. As can be seen from Table 5.1, the crack is detected at 1.76in that is within 4% of the actual location. The first two mode shapes are used for locating the crack in Case 7 but an additional mode shape is required in Case 8 (mode shape y1), as identified by the algorithm. This can be attributed to the fact that the crack orientation of 85^o is essentially a Mode-I crack whereas the orientation of 45^o exhibits a significant Mode-II content but its contribution to severity of the crack is relatively lower than Mode-I. Also, the third natural frequency ratio which is found to be most sensitive to damage exhibits a slightly higher drop in Case 8 than Case 7. These damage detection parameters clearly show that crack orientation can influence the identification of damage location as well as damage severity.

Various crack locations within members 4 and 6 are also used to investigate the capability of the algorithm to locate damage within a feasible region. Cases in which the crack is introduced at 4.6in show the predicted crack location to be within 1.1%. However, some other cases with the crack located closer to the ends at 1.4in and 7.6in

show a higher error in detecting crack location. In general, it is observed that cracks located close to the joints (around 15% of the member length) are hard to detect. This is a limitation of the proposed approach and needs to be investigated further in future research. This has been observed in the existing literature as well, Fan and Qiao [1] found that wavelet transform methods are commonly unable to detect cracks near the boundaries because they detect discontinuities due to end effects that can result in multiple peaks. Using filtering windows is not enough to attenuate these peaks since the filter does not distinguish between the peaks resulting from the discontinuity and those resulting from the end effects.

5.1.2. Warren Truss – 23 Members

The Warren truss shown in Figure 5.1b is the second example used to examine the capability and overall robustness of the damage detection algorithm. The numbering system for identifying the truss members is similar to the previous example with the bottom members numbered from left to right as 1-6, the top members as 7-11, the right-leaning members as 12-17, and the left-leaning members as 18-23. Damage is introduced in three truss members, namely 7, 12, and 14, as shown in Figure 5.1b. The damage is introduced in one member at a time in the six different cases presented in Table 5.2. Wavelet transform results are also presented for some of the cases to illustrate the effect of increasing number of truss members and the location of the damaged members. The numerical and wavelet results presented in the previous section are also discussed here to emphasize the findings and observations from this section.

Table 5.2: Results of Warren Truss - 23 Members, Six Cases with Three Damaged Members (Crack Size: 0.07in)

Warren Truss Parameters					Results			
Case #	Member ID	Member orientation (deg.), θ	Crack orientation (deg.), β	Actual location (in), l_a	Predicted location (in), l_c	Error %	Mode shapes	Natural frequency ratio, ω_n'
1	7	60	60	4.6	4.50	1.1	x1,x2,x3	ω_3, 0.998
2	7	45	45	7.6	7.43	1.9	x1,x2,x3	ω_2, 0.998
3	12	60	60	1.4	1.76	4.0	X2,y2,x3,y3	ω_3, 0.998
4	12	60	60	4.6	4.50	1.1	all	ω_3, 0.998
5	14	60	45	7.0	7.08	0.9	y1,x2,y2,x3,y3	ω_3, 1
6	14	60	60	2.0	2.34	3.9	y1,x2,y2,x3,y3	ω_2, 1

In Table 5.2, Case 1 and Case 4 are identical to Case 1 and Case 5 in Table 5.1 so as to demonstrate the influence of the increasing number of truss members on the damage detection technique. Location of members 4 and 6 in Figure 5.1a is respectively identical to the location of members 7 and 12 in Figure 5.1b. The results are, therefore, found to be identical, but natural frequency ratios corresponding to the most sensitive modes for damage show a slightly smaller drop in comparison to the ratios obtained for the cases in Table 5.1. The wavelet transform results can reveal more information with regard to varying number of truss members that cannot be obtained from numerical results. For instance, the wavelet plot of mode shape x1 in Figure 5.8, for Case 1 (in Table 5.2), shows a significant drop in the coefficient amplitude as compared to Figure 5.2 (Case 1 from Table 5.1), but the peak caused due to the singularity is still clearly visible. It can be concluded that the top members are not significantly influenced by an increasing number of truss members. On the other hand, the wavelet plot of the inclined member, member 12, shows more side-peaks in Figure 5.9 than the number of peaks observed in Figure 5.5 (Case 5 from Table 5.1), indicating that the end effects contribute significantly.

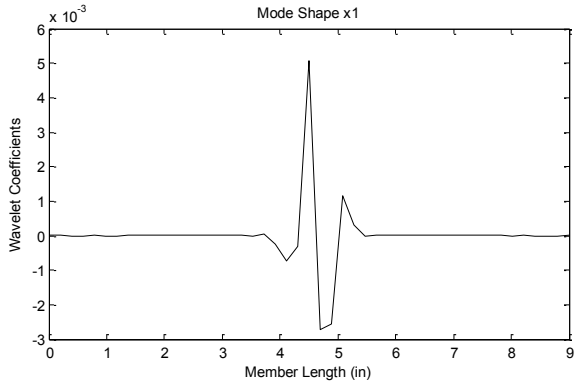

Figure 5.8: Wavelet Coefficients of Mode Shape x1 (Case 1, Table 5.2).

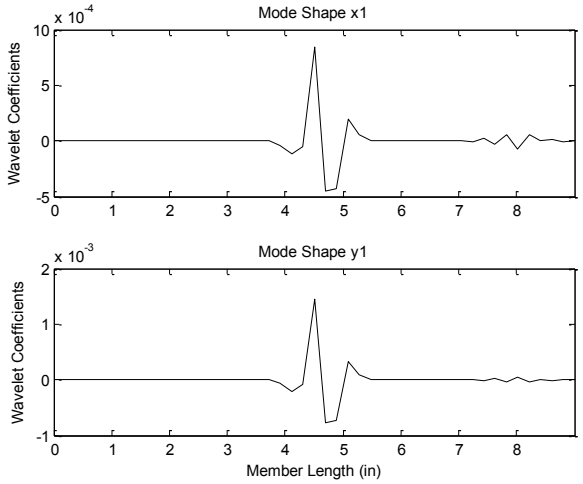

Figure 5.9: Wavelet Coefficients of Mode Shape 1 (Case 4, Table 5.2).

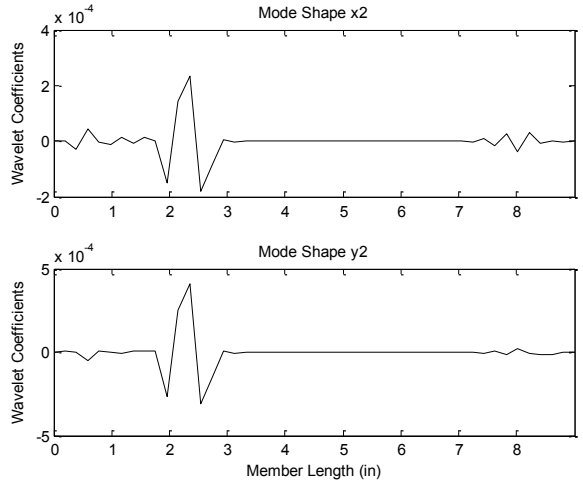

Figure 5.10: Wavelet Coefficients of Mode Shape 2 (Case 6, Table 5.2).

Another observation from Figures 5.5 and 5.9 is that the end effects caused by the free joint tend to suppress the end effects resulting from the fixed joint.

In Case 6, a mixed-mode crack is introduced in member 14 (an inner inclined member) that is located 2in from the left joint of the member. The wavelet coefficients of the second mode are plotted in Figure 5.10. As can be seen from Figure 5.10, there are multiple side-peaks resulting from end effects that could lead to difficulties in detecting damage. This can be attributed to the general challenge in detecting mixed-mode cracks and damage in inclined members and has been reported in the existing literature [25]. Pothisiri and Hjelmstad [25] found that detecting damage in inclined members is more challenging as compared to horizontal members, and developed an algorithm based on optimization that was not completely successful in detecting damage in inclined members in the presence of noise. It can be discerned from the results that by increasing the number of truss members, random noise is expected to add to the signal response causing difficulty in detecting damage with high accuracy in the inner inclined members of the truss. Furthermore, the noise generated by varying this parameter has been found to render the first mode shape as an outlier for the algorithm developed in this study.

5.2. Howe Truss Structures

This section presents simulation results of a Howe truss that has been used to further test the capability of the algorithm presented in Chapter 4. This example is also used to enhance the understanding of some of the model parameters discussed in Section 5.1. Figure 5.11 shows two Howe truss structures with 21 members and 45 members respectively. The truss members shown in Figure 5.11 have identical geometry and material properties to the ones presented in Figure 5.1. The length of the

inclined members and the vertical members (height of the structure) is a function of the truss orientation, θ, and the length of bottom and top members, l.

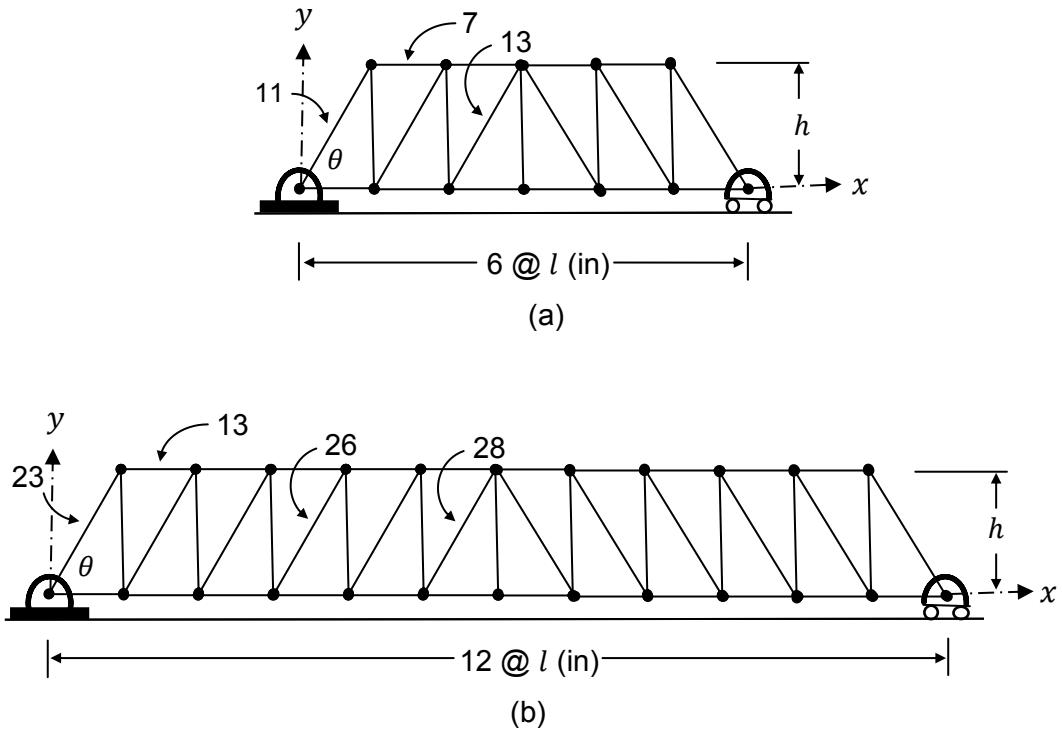

Figure 5.11: (a) Howe Truss – 21 Members with Three Damaged Members. (b) Howe Truss – 45 Members with Four Damaged Members.

5.2.1. Howe Truss – 21 Members

The Howe truss structure shown in Figure 5.11a has 21 members with three damaged members. The bottom and top members are identified by the same numbering system that is used in Section 5.1, with the bottom and the top members numbered from left to right as (1-6) and (7-10) respectively. For all inclined members, the numbering continues from left to right as 11-16 and for vertical members as 17-21. Three damaged members, namely 7, 11, and 13 are investigated for damage detection of the structure by studying six cases presented in Table 5.3. The length of the damaged members is fixed at 9in by correspondingly varying truss orientation and the length of bottom and top members.

Table 5.3: Results of Howe Truss - 21 Members, Six Cases with Three Damaged Members (Crack Size: 0.07in).

Howe Truss Parameters					Results			
Case #	Member ID	Member orientation (deg.), θ	Crack orientation (deg.), β	Actual location (in), l_a	Predicted location (in), l_c	Error %	Mode shapes	Natural frequency ratio, ω_n'
1	7	60	60	4.6	4.50	1.1	x1,x2,x3	ω_1, 0.999
2	7	45	45	7.6	7.67	0.7	x1,x2,x3	ω_1, 0.999
3	11	60	60	2.0	2.34	3.9	all	ω_2, 0.994
4	11	60	60	4.6	4.50	1.1	all	ω_1, 0.995
5	13	60	45	7.0	6.85	1.6	y1,x2,y2,x3,y3	ω_3, 0.995
6	13	60	60	1.4	1.76	4.0	y1,x2,y2,x3,y3	ω_2, 0.994

As can be seen from Table 5.3, the damage introduced at different locations along the member length can be detected within 4% of actual damage location using the damage detection algorithm presented in Chapter 4. Natural frequency of the damaged Howe truss structure corresponding to the most sensitive mode for damage detection shows an insignificant drop in natural frequency ratios (Case 1 and 2 in Table 5.3). It may be noted from the results in Table 5.3 that all natural modes are reported to be sensitive to damage at least once in the study cases, whereas the Warren truss in Section 5.2 exhibited least sensitivity for the first vibrational mode. The first three mode shapes in x-axis global coordinate are required to detect the damage in the top members, this is similar to the results of the Warren truss. As can be observed in Cases 3 through 6 from Table 5.3, the algorithm requires one less mode to identify the damage location in member 13 than in member 11 for the same damage characteristics, indicating some difficulty in damage diagnostics associated with inner inclined members. The errors associated with damage detection in Case 2 indicates that damage closer to the boundaries may not be as challenging in the Howe truss as compared to the Warren truss. However, the wavelet plots in Figure 5.12 and Figure 5.13 reveal that the

algorithm will still have difficulty in both types of structures to distinguish between the peaks caused by damage and the side peaks caused by the end effects. But it can be seen from wavelet results of Howe and Warren truss structures that the amplitude of side-peaks observed in the wavelet plots of the Howe truss is relatively smaller than the ones observed for the Warren truss (refer to Case 4 and Case 6 from Table 5.2 for comparison).

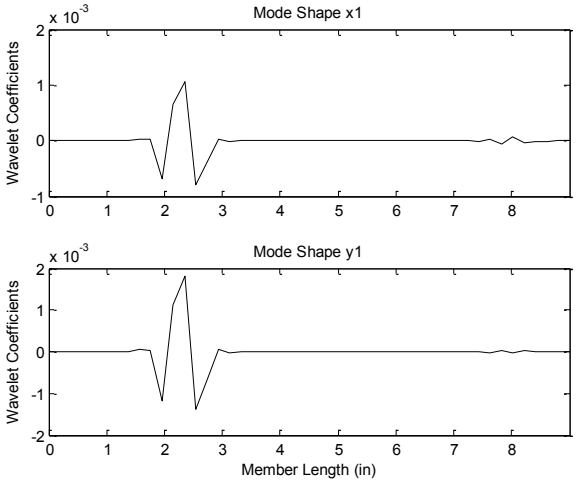

Figure 5.12: Wavelet Coefficients of Mode Shape 1 (Case 3, Table 5.3).

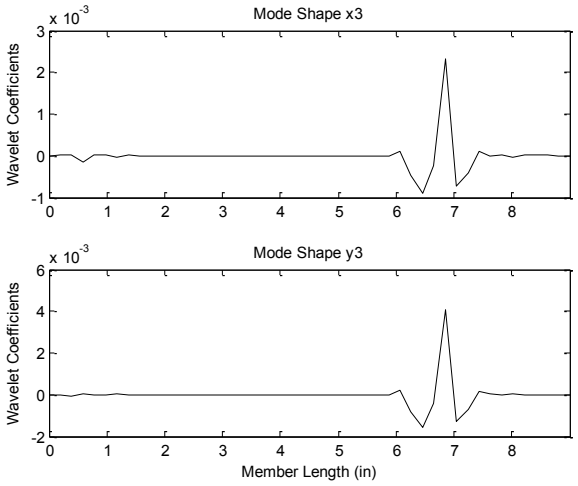

Figure 5.13: Wavelet Coefficients of Mode Shape 3 (Case 5, Table 5.3).

Wavelet results of Case 3 and Case 5 show a clear detection of discontinuity at the predefined crack location, as can be seen in Figure 5.12 and Figure 5.13. The side peaks are filtered out to a reasonable extent while preserving good localization accuracy of the main peak. Even though the crack is introduced close to the connecting joint of the truss member, the main peak can still be easily discerned, resulting in a noise-free wavelet plot. Most of the other characteristics resulting from varying model parameters observed in the Warren truss have also been found in the analysis of the Howe truss.

5.2.2. Howe Truss – 45 Members

In this example, the number of truss members is increased to 45 in order to comprehend the influence of increased complexity on the damage detection algorithm. Figure 5.11b illustrates the location of four damaged members, namely 13, 23, 26, and 28 in the Howe truss structure that is used for analysis. Location of these members is selected so as to understand the influence of member location within the structure, and to investigate the results due to damage in the inner inclined member in the truss. Truss member numbers are identified as follows: top members (1-12), bottom members (13-22), inclined members (23-34), and vertical members (35-45). In Table 5.4, eight cases are presented with damage introduced in four members at different locations. Wavelet transform plots are also produced to examine the influence of the increasing number of truss members in the Howe truss structure.

Table 5.4: Results of Howe Truss - 45 Members, Eight Cases with Four Damaged Members (Crack Size: 0.07in)

Howe Truss Parameters					Results			
Case #	Member ID	Member orientation (deg.), θ	Crack orientation (deg.), β	Actual location (in), l_a	Predicted location (in), l_c	Error %	Mode shapes	Natural frequency ratio, ω_n'
1	13	45	60	4.6	4.50	1.1	x1, x2,x3	ω_2, 0.999
2	13	30	60	7.6	7.67	0.7	x1, x2,x3	ω_3, 0.999
3	23	60	45	4.6	4.50	1.1	all	ω_3, 0.997
4	23	60	45	2.0	2.35	3.9	all	ω_3, 0.997
5	26	60	60	7.0	6.85	1.7	all	ω_2, 0.998
6	26	60	45	2.0	2.35	3.9	y1,x2,y2,x3,y3	ω_2, 0.999
7	28	60	45	1.4	1.46	0.7	x1,y2,x3,y3	ω_3, 0.997
8	28	60	60	7.0	6.85	1.7	y1,x2,y2,x3,y3	ω_3, 0.998

The results of Case 2 and Case 7 from Table 5.4 demonstrate the capability of the algorithm to detect damage effectively in the feasible region, approximately 15% (of member length) beyond the boundaries even with the increasing number of truss members. In addition, the error associated with the predicted damage location is found to be within 4%. It can be clearly noted from results in Table 5.4 that fewer mode shapes are required to detect a crack with the same characteristics as the damaged member location changes from member 23 to member 28. This could be attributed to the fact that the signal-to-noise ratio decreases in the modal response as the damaged inclined member is located closer to the middle of the structure. Thus, wavelet results of Cases 4, 5, 6 and 8 are presented in Figures 5.14 through 5.17 for some of the mode shapes used for damage detection. The wavelet results for identical damage characteristics introduced at two different locations, 2in and 7in within the member length, reveal that the mode shapes of member 26 exhibit higher noise-to-signal characteristics due to end effects as compared to the mode shapes of members 23 and 28. It can be concluded that some inclined members may require more attention during damage detection, and

the structural simulation of a damaged structure may be a good starting point to identify these members. Additionally, it can be discerned that there is a direct correlation between an increasing number of truss members and an increasing noise-to-signal amplitude. Even though wavelet results of member 23 in Figure 5.14 and member 11 in Figure 5.12 (Case 3 from Table 5.3) exhibit damage discontinuity at the same location, wavelet results of member 23 exemplify the influence of an increasing number of truss members as the side peaks become more apparent than in wavelet results of member 11 for the same damage characteristics.

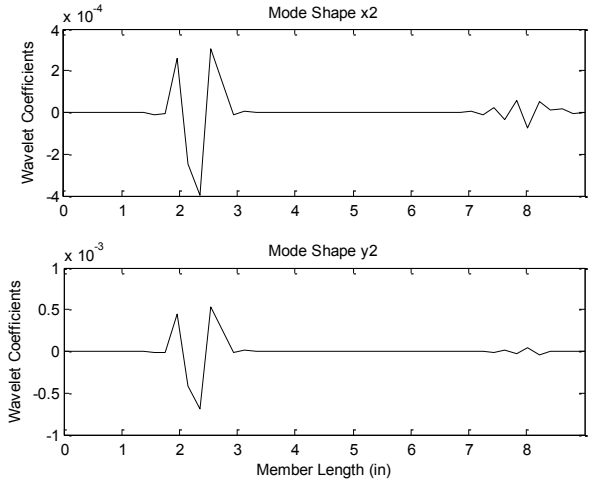

Figure 5.14: Wavelet Coefficients of Mode Shape 2 (Case 4, Table 5.4).

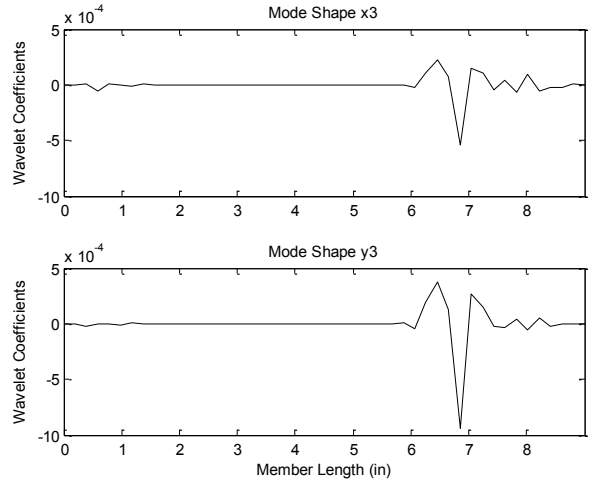

Figure 5.15: Wavelet Coefficients of Mode Shape 3 (Case 5, Table 5.4)

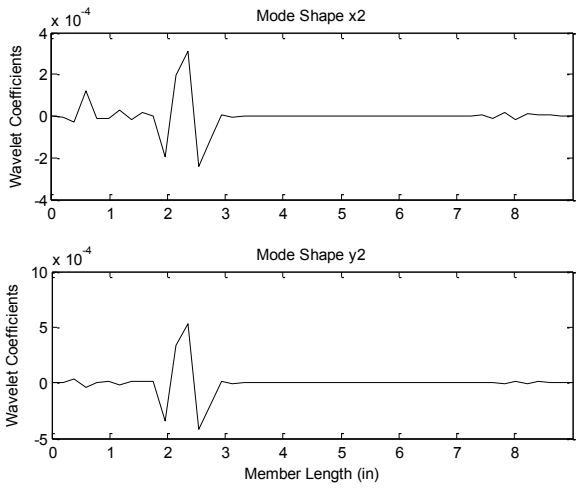

Figure 5.16: Wavelet Coefficients of Mode Shape 2 (Case 6, Table 5.4)

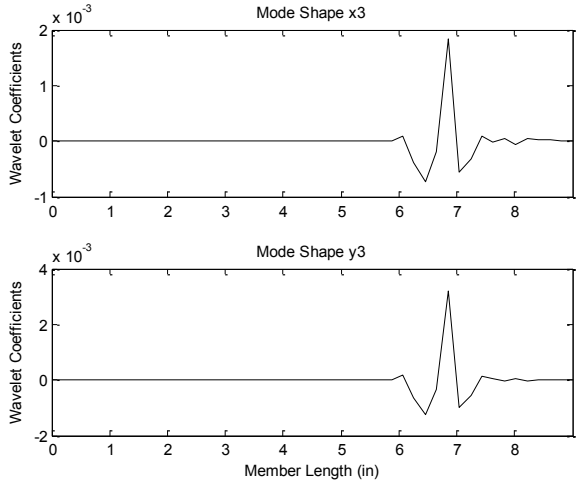

Figure 5.17: Wavelet Coefficients of Mode Shape 3 (Case 8, Table 5.4)

It may be noted that most of the observations with regard to the varying model parameters in Howe truss structures have also been observed in Warren truss structures. However, there are some distinctions between the results of the two structures. By comparing contaminated wavelet results (Figure 5.10 and Figure 5.16) from Warren truss and Howe truss respectively for identical damage characteristics and damage location, the signal-to-noise ratios in these plots are very close although the difference in number of truss members associated with each truss structure is large. This could be attributed to the fact that the ratio of the mass of a structure to the area

occupied by the structure is higher for Howe truss, allowing it to have lower natural frequencies. Thus, it can be concluded that the influence of increasing the number of truss members has more effect on damage diagnostics of Warren truss structures than on Howe truss structures. Additionally, natural frequency ratios corresponding to the most sensitive mode to damage are often below unity in Howe truss structures whereas some cases of Warren truss have been found to have a natural frequency ratio of 1, indicating that the geometry of Howe truss plays a significant role in the overall results of damage detection. It can be concluded that the geometry of a structure could be favorable for damage diagnostics especially when the structure is more compact leading to a lower noise-to-signal ratio of the modal response signal, and a higher change in the frequency ratio.

5.3. Evaluating Damage Severity

Using the change in natural frequency ratio as a global damage sensitivity parameter, and for evaluating damage severity has not been found to be viable in this study. This is particularly true when the truss structure becomes large and complex. As can be seen from the results for four truss structures presented herein, the natural frequency ratios associated with the damage cases are either unity or very close to unity, indicating little change in frequencies after the introduction of damage. Furthermore, the natural frequency ratios corresponding to the most sensitive vibrational mode to damage have been found to be inconsistent. Therefore, damage severity is instead evaluated qualitatively from the correlation between crack size and the maximum amplitude of the wavelet coefficients. To assess the damage severity in a qualitative sense, at least two measurements with different levels of crack severity are required so as to compare the maximum amplitude of wavelet coefficients at the same crack location. Wavelet coefficients versus crack size of the first three mode shapes are

obtained with a propagating mixed-mode crack that grows from an initial size of 0.07in to 0.19in at an increment of 0.02in as shown in Figures 5.18, 5.19, and 5.20. The crack oriented at 45^o is located at 2.8in on member 6, member 7 and member 11 of the truss shown in Figure 5.1a and Figure 5.11a respectively. The structures containing these three members are oriented at 60^o.

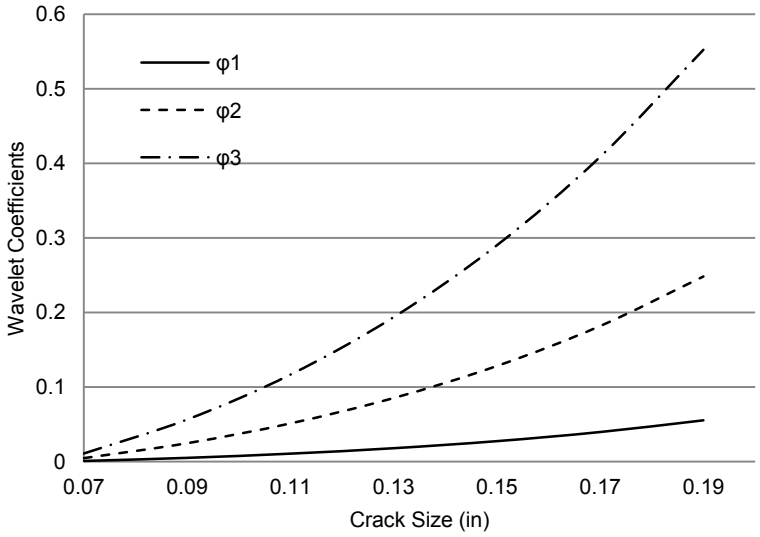

Figure 5.18: Wavelet Coefficients of First Three Mode Shapes versus Crack Size (Member 6, Figure 5.1a).

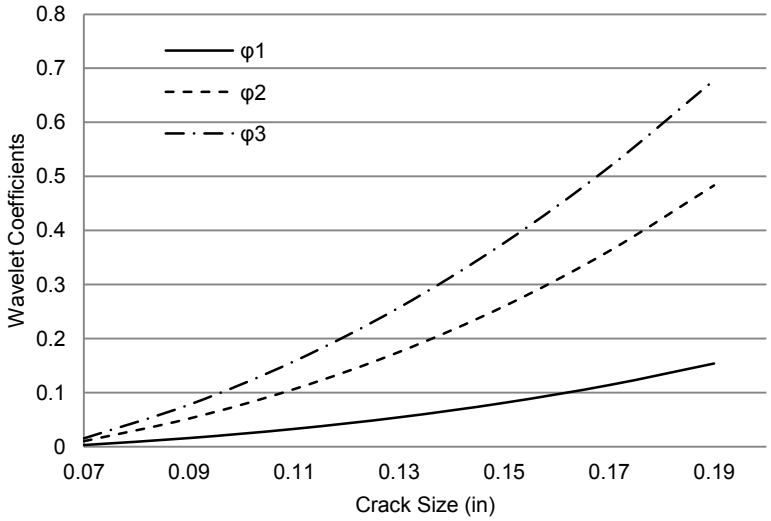

Figure 5.19: Wavelet Coefficients of First Three Mode Shapes versus Crack Size (Member 11, Figure 5.11a).

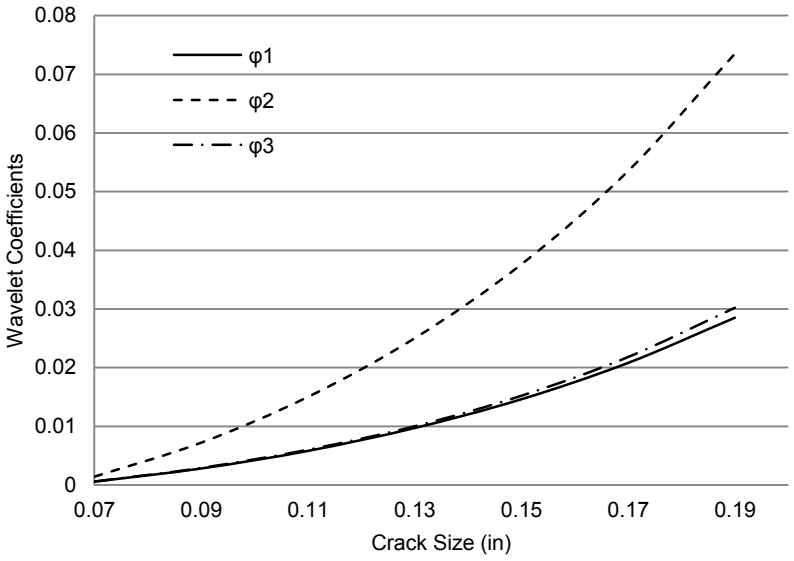

Figure 5.20: Wavelet Coefficients of First Three Mode Shapes versus Crack Size (Member 7, Figure 5.11a).

The amplitude of wavelet coefficients of the first three mode shapes in these figures further validates the conclusion that the geometry of the Howe truss presents an advantage over the geometry of the Warren truss, as far as damage detection is concerned. Thus, the overall results of the Howe truss structure are less contaminated by noise even with a larger number of truss members. Also, Figures 5.18, 5.19 and 5.20 confirm the observation that mode shape 1 is least sensitive to damage, therefore making it most vulnerable to noise due to end effects. On the contrary, the third mode shape is found to yield reliable results for damage detection with a minimal presence of noise when the damage is introduced in the Warren truss structures or in the inclined members of the Howe truss. The second mode shape is found to be more effective for the top members of Howe truss structures. It can be noted from Figure 5.20 that the coefficients for mode shape 2 increase significantly as the crack size increases, whereas the coefficients for mode shapes 1 and 3 exhibit a relatively small change.

5.4. Conclusions

This chapter presents the application of the damage detection algorithm that uses the wavelet transform for detecting mixed-mode cracks in large truss structures. Warren and Howe truss structures are used and multiple cases are run with the damage introduced at multiple locations. For all the simulation results, the algorithm successfully predicts the crack location within 4.0% even in the presence of noise. Crack location is found to significantly affect the accuracy of detection especially when the crack is located close to the boundaries. It can be concluded that the proposed algorithm is consistent and reliable when the crack location is reasonably beyond the joints, by about 15% of the member length.

The number of truss members is found to have a significant influence on damage detection since noise effects increase correspondingly. It can be concluded that as the number of truss members increases, the first mode shape becomes increasingly difficult to use for diagnostics. Additionally, an increasing number of truss members leads to unnoticeable changes in natural frequency even as the damage keeps propagating. Therefore, the use of natural frequency as a global measure of damage detection is not feasible. Damage severity has been evaluated qualitatively from the relationship between crack size and the magnitude of the wavelet coefficients. Damage detection is found to be more challenging in inclined members, thereby making truss orientation an important parameter in damage detection. The application of wavelets is found to be more successful with Mode-I dominant cracks as compared to mixed-mode cracks.

Through a comparison of the results between Warren truss and Howe truss structures, it is found that the geometry of a structure is an important property that can influence damage detection. The Howe truss structures are found to have less contaminated wavelet results, and a relatively higher drop in natural frequency ratios as

compared to similar Warren truss structures. The third natural mode shape is often associated with large amplitudes of wavelet coefficients when the damage is introduced in Warren trusses, or in the inclined members of Howe truss structures. Damage in the top members of Howe truss structures can be reliably detected using the second mode shape. Thus, it can be concluded that higher modes are not often associated with higher sensitivity to damage, but that the most sensitive mode for damage is related to the geometry of the structure and location of the damaged member.

Chapter 6

Conclusions and Future Scope

This chapter presents the main findings and overall conclusions of this study. The conclusions include a discussion on the model developed for representing the mixed-mode crack as well as the finite element modeling performed for analyzing damaged trusses. Possible improvements and validation as well as future scope are also discussed in this chapter.

6.1. Conclusions

The macroscopic model of a mixed-mode crack integrated with the finite element model, developed in Chapter 3, has been found to be reasonably successful in representing damage in axially loaded bars and truss structures investigated in this study. However, the direct use of structural modal properties has met with limited success for the purposes of damage detection. The ratio of natural frequency change may be used as a parameter to evaluate the severity of damage by using the difference between undamaged and damaged natural frequency of a structure. But it has been found in this study that the natural frequency-based method is unreliable for damage detection in large and complex structures such as the Warren truss and the Howe truss. This can be attributed to the fact that the natural frequency is a global parameter and exhibits limited sensitivity to local events such as cracks, especially when the crack size is relatively small. It can be concluded that the sensitivity of natural frequency to damage depends significantly on the size of damage and the dimensions of the overall structure.

The direct use of mode shapes in damage detection requires the vibrational modes to exhibit a significant difference between the undamaged and the damaged structure. These mode shapes can be used to locate the damage since they are considered to be

more sensitive to local events as compared to natural frequencies. In this study, the use of mode shapes is found to be acceptable for damage detection only when the damaged structure is simple, and when the crack size is relatively large. Mode shapes can be vulnerable to noise and may require a significant amount of data collection in order to avoid problems with coarse sampling. Furthermore, it is observed that there are some regions where it is extremely challenging to detect a damage even if multiple vibration modes are used. This can be caused by the presence of nodes associated with the mode shapes, or boundary conditions, or the specific orientation of structural members. These issues are particularly relevant in large and complex structures. Therefore, the use of mode shapes has been enhanced by using a signal processing technique, namely the wavelet transform, in this study to improve the capability of damage detection.

The shortcomings associated with the direct use of mode shapes have resulted in proposing an algorithm that is based on using the wavelet transform in order to extract relevant information from the vibration modes that can be directly related to specific damage characteristics. After investigating several wavelet families and their related parameters, the damage detection algorithm developed in this study for truss structures is found to yield reliable and robust results by using Sym4 (from the Symlet family). This wavelet is found to provide an effectively sharp spatial resolution with minimal edge effects, particularly by using a scale factor of 2 and 4 vanishing moments. The use of the Kaiser filtering window is found to enhance the capability of the spatial wavelet transform, and also significantly reduce the undesirable effects without compromising the determination of the feasible region for damage detection. Incorporation of statistical measures into the damage detection algorithm has yielded good results with an enhancement of the overall quality of the detection technique, and an improvement in the confidence level of the reported damage location. The application of the algorithm to

the damaged triangular truss structure has been found to be successful even after changing multiple model parameters. The normalized error associated with all the cases investigated for the triangular truss is found to be less than 3%. This confirms that the algorithm is capable of reliably localizing damage by using the maximum absolute value of the wavelet coefficients.

The application of the damage detection algorithm in Warren truss and Howe truss structures resulted in errors of up to 4%, using varying damage characteristics and geometrical properties over multiple simulations. The accuracy of damage detection is found to be very sensitive to crack location, especially when the damage is introduced near the connection joints in a truss. This observation is made in multiple simulation results, leading to the proposal of a feasible region over which the damage detection algorithm can successfully detect damage. Likewise, damage detection is found to be more challenging in some inclined members of the truss than the others, leading to the conclusion that some members are more sensitive to damage than others.

The simulation results reveal that the Howe truss is generally associated with higher SNR values as compared to the Warren truss. Additionally, the results from varying crack orientations indicate that the sensitivity of the modal properties is higher for purely Mode-I cracks than mixed-mode cracks. Wavelet coefficients at a detected damage location are found to give a strong indication of damage severity, allowing these coefficients to be used for evaluating the severity of damage qualitatively. However, a specific mode order is found to be more sensitive to damage, and highly effective to evaluate the damage severity at certain regions of a structure. Therefore, it can be concluded that higher modes are not often associated with higher sensitivity to damage, but the mode sensitivity to damage depends on the geometry of the structure and the location of the damaged member within the truss. The number of truss members is found to be an important parameter that can significantly influence the resolution of the

spatial wavelet transform by decreasing the SNR value, consequently affecting the accuracy of damage detection. It is observed that the noise associated with this parameter can cause the first mode shape to be considered as an outlier. In general, the model parameters investigated in this study are found to be very influential in the process of damage identification.

In summary, the research questions identified in Chapter 1 can be answered as follows:

1. Mixed-mode cracks do not exhibit as much influence over model parameters as purely Mode-I cracks. This makes it more challenging to detect mixed-mode cracks by using modal properties. Mixed-mode cracks are also more challenging to model, a macroscopic model has been developed in this study that has been successful in capturing the characteristics of an open crack.

2. It is not viable to use natural frequencies as a diagnostic tool for truss structures. Mode shapes, however, can be used for diagnostics by making use of the wavelet transform. In the truss structures analyzed in this study, multiple parameters such as geometry of the truss, number of truss members, crack size, crack orientation, etc. are found to influence damage detection with varying degrees of significance. Although a relatively coarse sampling of natural modes has been used for most of the simulations carried out in this study, the suitability of the algorithm needs to be investigated for sensitivity to natural mode sampling.

3. A damage diagnostic algorithm has been proposed in this study that can be applied to large and complex truss structures with mixed-mode cracks or purely Mode-I cracks. The noise effects and end effects are mitigated in the algorithm by an appropriate choice of a filtering window. Parameters associated with the filtering window need to be selected judiciously in order to balance the need of mitigating end effects and noise effects with the need to detect the change in vibrational modes.

6.2. Future Research

A logical subsequent step for this study is to verify the outcomes and validate the capability of the proposed damage detection algorithm through experimental testing. A truss structure of moderate complexity can be built and tested in the laboratory with pre-defined damage locations. The experimental work will specifically allow the algorithm to be tested for noise effects and data collection inaccuracies. Furthermore, the experimental work can also test the limitations of the algorithm to coarse sampling of natural modes. The experimental analysis will focus on studying the influence of the model parameters and other significant parameters that were seen to influence the performance of the damage detection technique from simulation results. Another possible parameter that can also be included in the analysis is the influence of multiple cracks with various crack orientations in a structural member or in different members simultaneously. The influence of these cracks can be investigated to further comprehend the capability of the modal response in damage detection.

The application of the algorithm developed in this study requires the measurements of mode shapes to evaluate the status of a structure and to locate possible damage. A precursor to the use of the proposed algorithm that can serve as a global damage detection model would be worthwhile in order to reduce the cost associated with the implementation process of laying instrumentation for data collection, especially in large structures. Furthermore, augmenting the capability of the algorithm to quantify the damage severity would allow the algorithm to estimate the remaining useful life of the structure at a given time.

One possible means of overcoming some limitations of the damage model developed in this study is by using alternative modeling techniques such as the cohesive zone model. The cohesive zone model can be used to simulate damage due to the

mixed-mode crack since this technique has been reported to exhibit major advantages over the conventional model based on LEFM [43]. The characteristics of the detected damage can also be expanded to include a breathing crack (opening and closing) instead of an open crack used in this study. The investigation of mixed-mode cracks can include other mixed modes such as a combination of Mode-I and Mode-III as well as a combination of Mode-II and Mode-III.

Alternative signal processing methods can be investigated so as to determine more ways of detecting discontinues within larger feasible regions on large and complex structures. If possible, such methods could be integrated into the algorithm proposed in this study. For example, the Hilbert-Huang transform (HHT) is one such option that has been used recently for some damage detection work. HHT has been found to be particularly well-suited for nonlinear and non-stationary data, and has been found to be highly efficient [44]. The use of the extended finite element method (XFEM) is also a favorable approach that can be used for modeling crack propagation. XFEM is known to retain the advantages of the classical FE method [45] while at the same time allowing a capability to model damage without a need to perform any remeshing.

In conclusion, nondestructive examination or evaluation (NDE) methods including modal properties-based methods are considered to be complimentary. For example, a visual inspection method may be used first to define the damage region, followed by an acoustic emission test to provide more details about the damage characteristics. Similarly, while using modal properties for damage detection, natural frequency sensitivity may also be used to identify the status of the structure in conjunction with other inspection methods. It can be confidently stated that there is no single method at this stage that can claim to identify all damage scenarios for any type of damage in any type of structure. However, with enhanced data-processing capabilities and more

research, many advances can be expected in the field of damage diagnostics in the near future.

REFERENCES

[1] Fan, W., Qiao, P., 2011, "Vibration-based Damage Identification Methods: A review and comparative study," *Structural Health Monitoring*, Vol. 10, pp. 83-111.

[2] Doebling, S.W., Farrar, C.R., Prime, M.B., Shevitz, D.W., 1996, "Damage Identification and Health Monitoring of Structural and Mechanical Systems From Changes in Their Vibration Characteristics: A Literature Review," Los Alamos National Laboratory, Report No. LA-13070-MS.

[3] Matzkanin, G., 2006, "Selecting a Nondestructive Testing Method: Visual Inspection," AMMTIAC Quarterly, Vol. 1, pp. 15-17.

[4] Bens, K., Wipf, T., Klaiber, F., 1997, "Review of Nondestructive Evaluation Techniques of Civil Infrastructure," *Journal of Performance Constructed Facilities*, Vol. 11, pp. 152-160.

[5] Wilcox, P., Lee C.-K., Scholey, J., Friswell, M., Wilson, M., Drinkwater, B., 2006, "Quantitative Structural Health Monitoring Using Acoustic Emission, Smart Structures and Integrated Systems," Proc. of SPIE, Vol. 6173K 1-10.

[6] Mian, A., Han, X., Islam, S., Newaz, G., 2004, "Fatigue Damage Detection in Graphite/Epoxy Composite Using Sonic Infrared Imaging Technique," *Composite Science and Technology*, Vol. 64, pp. 657-666.

[7] Peng, G., Yuan, S-H, 2005, "Damage Localization on Two Dimensional Structure Based on Wavelet Transform and Active Lamb Wave-based Method," *Material Science Forum*, Vols. 475-479, pp. 2119-2122.

[8] Giurgiutiu, V., 2008, *Structural Health Monitoring with Piezoelectric Wafer Active Sensors*, Elsevier Inc., Burlington, MA.

[9] Salawu, O. S., 1997, "Detection of Structural Damage through Changes in Frequency: A Review," *Engineering Structures*, Vol. 19, pp. 718-723.

[10] Cawley, P. and Adams, R. D., 1979, "The location of Defects in Structures from Measurements of natural frequencies," *Journal of Strain Analysis*, Vol. 4, pp. 49-57.

[11] Stubbs, N., Osegueda, R., 1990, "Global Damage Detection in Solids-Experimental Verification," *Journal of Analytical and Experimental Modal Analysis*, Vol. 5, pp. 81-97.

[12] Rizos, P. F., Aspragathos, N., Dimarogonas, A. D., 1990, "Identification of Crack Location and Magnitude in a Cantilever Beam from the Vibration modes," *Journal of Sound and Vibration*, Vol. 138, pp. 381-388.

[13] Chondros, T. G., Dimarogonas, A. D., 1998, "Vibration of a Cracked Cantilever Beam," *Journal of Vibration and Acoustics*, Vol. 120, pp. 742-746.

[14] Chondros, T. G., Dimarogonas, A. D., 2001, "Vibration of a Beam with a Breathing Crack," *Journal of Sound and Vibration*, Vol. 239, pp. 57-67.

[15] Dimarogonas, A. D., 1996, "Vibration of Cracked Structures: A State of the Art Review," *Engineering Fracture Mechanics*, Vol. 55, pp. 831-857.

[16] Liew, K.M., Wang, Q., 1998, "Application of Wavelet Theory for Crack Identification in Structures," *ASCE Journal of Engineering Mechanics*, Vol. 124, pp. 152-157.

[17] Surace, C., Ruotolo, R., 1994, "Crack Detection of a Beam Using the Wavelet Transform," *Proceedings of the 12th International Modal Analysis Conference*, pp. 1141-1145.

[18] Li, B., Chen, X.F., Ma, J.X., He, Z.J., 2004, "Detection of Crack Location and Size in Structures Using Wavelet Finite Element Methods," *Journal of Sound and Vibration*, Vol. 285, pp. 767-782.

[19] Pakrashi, V., Basu, B., O'Conner, A., 2007, "Structural Damage Detection and Calibration Using a Wavelet—Kurtosis Technique, *Engineering Structures*," Vol. 29, pp. 2097-2108.

[20] Kaul, S., 2014, "Crack Diagnostics in Beams Using Wavelets, Kurtosis and Skewness," *Nondestructive Testing and Evaluation*, Advance online publication, DOI:10.1080/10589759.2013.854783.

[21] Chang, C.-C., Chen, L.-W., 2005, "Detection of the Location and Size of Cracks in the Multiple Cracked Beam by Spatial Wavelet Based Approach," *Mechanical Systems and Signal Processing*, Vol. 19, pp. 139-155.

[22] Zhong, S., Oyadiji, S., 2007, "Crack Detection in Simply Supported Beams without Baseline Modal Parameters by Stationary Wavelet Transform," *Mechanical Systems and Signal Processing*, Vol. 21, pp. 1853-1884.

[23] Rucka, M., 2011, "Damage Detection in Beams Using Wavelet Transform on Higher Vibration Modes," *Journal of Technical and Applied Mechanics*, Vol. 49, pp. 399-417.

[24] Nair, K.K., Kiremidjian, A.S., 2005, "Derivation of a Damage Sensitive Feature Using the Haar Wavelet Transform," *Journal of Applied Mechanics*, Vol. 76, pp. 061015-1-9.

[25] Pothisiri, T., Hjelmstad, K.D., 2003, "Structural Damage Detection and Assessment from Modal Response," *Journal of Engineering Mechanics*, Vol. 129, pp. 135-145.

[26] Kim, H.M., Bartkowicz, T.J., 2001, "An Experimental Study for Damage Detection using Hexagonal Truss," *Computers and Structures*, Vol. 79, pp. 173-182.

[27] Weber, B., Paultre, P., 2010, “Damage Identification in a Truss Tower by Regularized Model Updating,” *Journal of Structural Engineering*, Vol. 36, pp. 307-316.

[28] Hao, H., M.ASCE, Xia Y., 2002, “Vibration-based Damage Detection of Structures by Genetic Algorithm,” *Journal of Computing in Civil Engineering*, Vol. 16, pp. 222-229.

[29] Ovanesova, A.V., Suarez, L.E., 2003, “Application of Wavelet Transforms to Damage Detection in Frame Structures,” *Engineering Structures*, Vol. 26, pp. 39-49.

[30] Wang, G-P., Hong, Y., Hong, D-P., 2008, “Damage Detection of Truss-Like Structures Using Wavelet Transforms,” *Modern Physics Letters B*, Vol. 22, pp. 1165-1170.

[31] Li, H., Yang, H., Hu, S.-L., 2006, “Modal Strain Energy Decomposition Method for Damage Localization in 3D Frame Structures,” *Journal of Engineering Mechanics*, Vol. 132, pp. 941-951.

[32] Stubbs, N., Kim, J. T., Farrar, C. R., 1995, “Field Verification of a Non-destructive Damage Localization and Severity Estimation Algorithm,” Proc., IMAC, Society for Experimental Mechanics, Bethel, Conn., 210-218.

[33] Tang, L., Luo, X., Liu, Z., Liu, Y., He, T., Fang, D., 2013, “Octonion Structural Response Vector and Potential Structural Damage Identification Method,” *Journal of Damage Mechanics*, Vol. 22, pp. 572-589.

[34] Anderson, T.L., 2004, *Fracture Mechanics: Fundamentals and Applications*, 3rd ed., CRC Press, FL.

[35] Tada, H., Paris, P.C., Irwin, G.R., 2000, *The Stress Analysis of Cracks Handbook*, 3rd ed., ASME Press, NY.

[36] Logan, D.L., 2012, *A First Course in Finite Element Method*, 5th ed., Cengage Learning, CT.

[37] Rao, Singiresu S. 2011, *Mechanical Vibrations*, 5th ed. Prentice Hall, N.J.

[38] Misiti M., Misiti Y., Oppenheim G., Poggi J-M., 2013, *Wavelet toolbox—User’s guide*, MathWorks, Natick, MA.

[39] Fugal, D., 2009, *Conceptual Wavelets in Digital Processing: An In-depth, Practical Approach for the Non-mathematician*, Space & Signals Technical Pub., San Diego, CA.

[40] MathWorks, 2013, *Signal Processing Toolbox—User’s guide*, Natick, MA.

[41] Du, K-L, Swamy, M.N.S., 2010, *Wireless Communication Systems: From Rf Subsystems to 4g Enabling Technologies*, Cambridge University Press, Cambridge, UK.

[42] MathWorks, 2010, *MATLAB User Guide*, Natick, MA.

[43] Elices, M., Guinea, G.V., Gomez, J., Planas, J., 2002, "The Cohesive Zone Model: Advantages, Limitations, and Challenges," *Engineering Fracture Mechanics*, Vol. 69, pp. 137-163.

[44] Huang, N. E., Shen, Z., Long, S. R., Wu, M. C., Shih, H. H., Zheng, Q., Yen, N. C., Tung, C. C., Liu, H. H., 1998, "The Empirical Mode Decomposition and the Hilbert Spectrum for Nonlinear and Nonstationary Time Series Analysis," *Proceedings of the Royal Society of London*, A. 454, pp. 903-995.

[45] Sukumar, N., Moes, N., Moran, B., Belytschko, T., 2000, "Extended Finite Element Method for Three Dimensional Crack Modeling," *International Journal Numerical Methods in Engineering*, Vol. 48, pp. 1549-1570.